NASA TECHNICAL NOTE

NASA TN D-3495

NASA TN D-3495

ANALYSIS OF TAILORED-INTERFACE OPERATION OF SHOCK TUBES WITH HELIUM-DRIVEN PLANETARY GASES

by William J. Loubsky and John O. Reller, Jr.

Ames Research Center
Moffett Field, Calif.

NATIONAL AERONAUTICS AND SPACE ADMINISTRATION • WASHINGTON, D. C. • JULY 1966

ANALYSIS OF TAILORED-INTERFACE OPERATION OF SHOCK TUBES WITH HELIUM-DRIVEN PLANETARY GASES

By William J. Loubsky and John O. Reller, Jr.

Ames Research Center
Moffett Field, Calif.

NATIONAL AERONAUTICS AND SPACE ADMINISTRATION

For sale by the Clearinghouse for Federal Scientific and Technical Information
Springfield, Virginia 22151 – Price $2.00

ANALYSIS OF TAILORED-INTERFACE OPERATION OF SHOCK TUBES WITH HELIUM-DRIVEN PLANETARY GASES

By William J. Loubsky and John O. Reller, Jr.

Ames Research Center

SUMMARY

The perfect-gas relations which determine the conditions for tailored operation of a shock tube are summarized, and a computer method for calculating real-gas effects is presented. The analysis incorporates the following assumptions: (a) the driver gas behaves as a thermally and calorically perfect gas; (b) the test gas is in thermodynamic equilibrium; and (c) viscous effects are neglected. Equations are derived that enable the determination of the time, τ, during which the reservoir properties remain constant (e.g., the time between the arrival of the incident shock wave and the arrival of the reflected expansion head at the end of the driven tube). It is shown that a maximum value for τ exists for a range of driven-to-driver tube length ratios; an optimum ratio is defined for minimum driver length at maximum τ. A minimum value for τ also exists if tailoring is to be achieved and corresponds to an allowable maximum component length ratio. Charts are presented which facilitate the determination of the tailored conditions for a constant area shock tube having a helium drive and air, CO_2, N_2, or A as test gases. Driver conditions are varied to include pressures from 10 to 1,500 atm and temperatures from 300° to 10,000° K. Substantial deviations from the perfect-gas results are found for tailored Mach numbers greater than 8. For a given reservoir or reflected-shock enthalpy, real-gas effects may reduce driver temperature requirements by 30 to 50 percent. Driver energy is reduced also, since real-gas effects enable the use of a shorter driver length. Steady-state times τ, however, can be substantially less than the perfect-gas values. Examples of the use of the charts are included.

INTRODUCTION

One factor that limits the test time available in a shock tunnel is the arrival at the nozzle entrance of the reflected driver expansion wave. One method of making this disturbance negligibly small (as illustrated in refs. 1 and 2) is to use a large volume driver section. This is not practical when energy requirements for the driver gas are so high that the driver gas must be arc-heated; the present state of the art makes it necessary for driver volumes to be quite small.

A second limitation on test time in a shock tunnel is the reflection of pressure waves from the interface of the driver gas and test gas.

Hertzberg et al. (ref. 3) were one of the first groups to report a method of eliminating these disturbances. The method was called the tailored-interface mode of operation and it was observed that test times per foot of driven tube should be approximately six times those for the reflected, nontailored condition. The technique consists in selecting an initial loading pressure in the driven tube for a given driver condition so that no downstream wave is generated when the reflected shock wave interacts with the driver gas interface. Ford and Glass reported (ref. 4) the basic interaction as early as 1954. Interface tailoring has since been studied by many groups. Flagg (ref. 5) provides a detailed analysis for perfect gases in which equations for the tailored shock Mach number are derived and results are presented for Mach numbers up to 8.

The purpose of the present report is to show the extent to which equilibrium real-gas considerations influence the tailored-interface condition for air and other test gases, as well as to provide information for general use in the preliminary design of facility components and experiments. A computer method is presented which extends the perfect-gas analysis to include real-gas effects when the test gas is in equilibrium. Charts are provided to enable the determination of the tailored-interface mode of operation for a constant area shock tube employing a helium driver and air, CO_2, N_2, and A as test gases. The range of driver temperatures considered is from 300° to 10,000° K and pressures from 10 atm to 1,500 atm; thus cold, resistance heated, and arc-heated drivers are included. From these charts and the gasdynamic charts in references 6 through 12, the shock tube flow and thermodynamic properties can be determined. Equations are derived which enable the determination of the available steady-state time in the reservoir as a function of the driver and driven tube lengths. The optimum and maximum component length ratios are derived. All results are presented in graphical form. The results indicate substantial deviations from the perfect-gas analysis.

In practice, various mechanisms for energy transfer, such as viscosity, radiation, and nonideal wave interactions, will reduce performance below the results presented herein, but their consideration is beyond the scope of the present report.

SYMBOLS

a sound speed

e internal energy per unit mass

h enthalpy per unit mass

L length

M shock Mach number

m molecular weight

p	pressure
R	gas constant of cold gas
T	temperature
t	time
U	flow speed relative to shock wave
u	flow speed relative to test facility
V	shock wave speed relative to test facility
x	coordinate length from diaphragm station
γ	ratio of specific heats
ρ	density
τ	steady-state time in the test gas reservoir

Subscripts

a	condition upstream of standing normal shock wave
b	condition downstream of standing normal shock wave
D	driver section
DT	driven tube section
L	limiting value
max	maximum value
min	minimum value
opt	optimum value
R	reflected shock wave
RHe	reflected shock wave in helium
RR	reflected shock wave from interface
S	incident shock wave

ST tailoring value of incident shock wave

TS reservoir test gas

1 condition ahead of incident shock wave in quiescent gas

2 condition behind incident shock wave

3 condition behind incident interface

4 condition in driver section prior to diaphragm breakage

5 condition behind reflected shock wave in the test gas

6 condition behind reflected shock wave in the driver gas when the interface is tailored

7 condition behind reflected shock wave in the driver gas when the interface is not tailored

8 condition behind the reflected shock wave from the interface when the interface is not tailored

Reference Constants

p_o 1 atm = 1.013×10^5 N/m^2

R_o 286.8 m^2/sec^2 ^oK for air; 296.9 m^2/sec^2 ^oK for N_2; 189.2 m^2/sec^2 ^oK for CO_2; 207.8 m^2/sec^2 ^oK for argon; 2078 m^2/sec^2 ^oK for He

T_o 273.16^o K

T_1 300^o K

ρ_o 1.290 kg/m^3 for air; 1.246 kg/m^3 for N_2; 1.960 kg/m^3 for CO_2; 1.780 kg/m^3 for argon

ANALYSIS

The tailored-interface condition exists, by definition, when no unsteady wave disturbance propagates into the shock tunnel reservoir as a result of the interaction of the reflected shock wave and the driver gas interface; that is, the interface is brought to rest by the reflected shock wave. The general flow process is illustrated in figure 1 with a physical schematic and distance-time diagram for a constant area shock tube. The interface is "tailored" when the pressure ratio $p_8/p_5 = 1.0$.

Perfect Gas Tailoring

In this report a thermally and calorically perfect gas is referred to simply as a perfect gas. The interaction of a shock wave with a contact surface (interface) is reported for a perfect gas in reference 4, and the criterion for tailoring is expressed in terms of the specific internal energy ratio

$$\frac{e_3}{e_2} = \frac{\dfrac{\gamma_4 + 1}{\gamma_4 - 1} + \dfrac{p_5}{p_2}}{\dfrac{\gamma_1 + 1}{\gamma_1 - 1} + \dfrac{p_5}{p_2}} \tag{1}$$

Flagg in reference 5 gives the tailoring requirement in terms of the temperature ratio T_3/T_2 by the expression

$$\frac{T_3}{T_2} = \frac{m_4(\gamma_4 - 1)\left(1 + \dfrac{\gamma_4 + 1}{\gamma_4 - 1}\dfrac{p_5}{p_2}\right)}{m_1(\gamma_1 - 1)\left(1 + \dfrac{\gamma_1 + 1}{\gamma_1 - 1}\dfrac{p_5}{p_2}\right)} \tag{2}$$

From equation (2), the tailoring requirement is satisfied by a unique temperature ratio across the incident interface for a specified gas combination and reflected shock pressure ratio.

The tailored shock Mach number, as illustrated in reference 5, for a shock tube of constant area can be found in terms of the diaphragm speed of sound ratio by a simultaneous solution of equation (2) and the following relations governing the flow process

$$\left.\begin{aligned}
\frac{T_2}{T_1} &= \left[\left(\frac{\gamma_1 - 1}{\gamma_1 + 1}\right)(M_S^2 - 1) + M_S^2\right]\left[\left(\frac{\gamma_1 - 1}{\gamma_1 + 1}\right)(M_S^2 - 1) + 1\right]\frac{1}{M_S^2} \\
\frac{T_3}{T_4} &= \left[1 - \left(\frac{\gamma_4 - 1}{\gamma_1 + 1}\right)\left(\frac{a_1}{a_4}\right)\left(M_S - \frac{1}{M_S}\right)\right]^2 \\
\frac{p_5}{p_2} &= \frac{(3\gamma_1 - 1)M_S^2 - 2(\gamma_1 - 1)}{(\gamma_1 - 1)M_S^2 + 2}
\end{aligned}\right\} \tag{3}$$

For purposes of this report the strong shock limit of the above relations is used. The error introduced by the approximation, which enables the tailored shock Mach number to be expressed in explicit terms, is less than a few percent for $M_{ST} > 6$. For the strong shock approximation the tailored shock Mach number can be expressed as

$$M_{ST} = \frac{a_4}{a_1}\left\{\frac{(\gamma_1 + 1)^2(\gamma_4 - 1) - [2\gamma_4(\gamma_1 - 1)(\gamma_4 + 1)(\gamma_1 + 1)^3]^{1/2}}{(\gamma_4 - 1)^2(\gamma_1 + 1) - 2\gamma_4(\gamma_1 - 1)(\gamma_4 + 1)}\right\} \tag{4}$$

and the tailoring requirement, equation (2), becomes simply

$$\frac{T_3}{T_2} = \frac{(\gamma_4 + 1)m_4}{(\gamma_1 + 1)m_1} \tag{5}$$

From equation (4) it is apparent that the tailored Mach number is only a function of the gas combination and the diaphragm speed of sound ratio.[1] When real-gas effects are considered, however, since the specific heats and degree of dissociation are functions of two thermodynamic properties, the tailored conditions in general as well as M_{ST} are also dependent upon the loading pressure p_1.

Real-Gas Tailoring

General considerations.- Real-gas effects such as variable specific heats, dissociation, and ionization preclude explicit relations, such as equations (1) to (5). In general, one must solve for the thermodynamic and flow properties downstream of the incident and reflected shock waves, and after the interaction of the reflected shock wave with the driver gas interface. In the present analysis thermodynamic equilibrium is assumed, and the thermodynamic gas models of Bailey and Lomax of the Ames Research Center are used (e.g., see ref. 13 for carbon dioxide). Each species is assumed to behave as an ideal gas. The species considered in each model are the following: (1) air: N_2, O_2, N, O, NO, N^+, O^+, NO^+, N^{++}, e^-; (2) nitrogen: N_2, N, N^+, N^{++}, e^-; (3) carbon dioxide: CO_2, CO, O_2, C, O, C^+, C^{++}, O^+, O^{++}, e^-; (4) argon: A, A^+, A^{++}, e^-.

The flow properties across the incident and reflected shock waves are governed by equations of conservation of mass, momentum, and energy and the equation of state:

$$\left.\begin{aligned} \rho_a U_a &= \rho_b U_b \\ p_a + \rho_a U_a^2 &= p_b + \rho_b U_b^2 \\ h_a + \tfrac{1}{2} U_a^2 &= h_b + \tfrac{1}{2} U_b^2 \\ \rho_b &= \rho_b(p_b, h_b) \end{aligned}\right\} \tag{6}$$

[1]Note that equation (4) differs from the general expression for shock tube Mach number by virtue of the added restraints imposed by the tailored condition.

The explicit form of the equation of state is determined from the assumed gas models.

The driver gas is assumed to be perfect and expanded isentropically by an unsteady expansion wave, the governing equation being

$$u_3 = \frac{2a_4}{\gamma_4 - 1}\left[1 - \left(\frac{p_3}{p_4}\right)^{\frac{\gamma_4 - 1}{2\gamma_4}}\right] \tag{7}$$

The validity of the perfect-gas assumption for a helium driver gas is based upon the fact that both electronic excitation and ionization are sufficiently small for the driver conditions investigated, to have a negligible effect on the thermodynamic properties. The results of reference 14 illustrate this point.

Computational procedure.- An IBM 7094 Fortran II computer program is used in the analysis, the input information being the conditions in the driver and driven tube sections before the diaphragm breaks. Equations (6) and (7) are solved simultaneously for the conditions behind the incident shock wave and in the fully expanded driver gas; the pressure and velocity are matched across the incident interface. The reflected shock properties are then found in a similar manner, with the condition that $u_5 = 0$. The input loading pressure p_1 is selected sufficiently low that the reflected wave from the driver-gas interface is a shock wave. Equations (6) are solved simultaneously for the conditions behind the transmitted shock wave in the driver gas and the reflected shock wave in the test gas, using the interface boundary conditions $u_7 = u_8$ and $p_7 = p_8$. The pressure ratio p_8/p_5 is then formed and a new loading pressure p_1 is determined from the equation $p_{1_{new}} = (p_8/p_5)p_{1_{initial}}$. The entire procedure, beginning with the incident shock wave, is repeated until the pressure ratio $p_8/p_5 < 1.005$. When this criterion occurs, the interface is considered to be tailored. The various forms in which the conservation equations are expressed in the procedure as well as the methods of iteration are presented in appendix A.

Component Lengths and Steady-State Time Relations

The purpose of tailored-interface operation is to achieve a maximum steady-state time, τ, in the test-gas reservoir. It can be shown that τ is a function of driver and driven tube lengths and that an optimum component length ratio $(L_{DT}/L_D)_{opt}$ exists for any given initial conditions in the driver and driven tube. This component length ratio is an optimum in the sense that it is the only ratio for which both the driver energy required is a minimum and τ is a maximum. This is best illustrated in the following sketches:

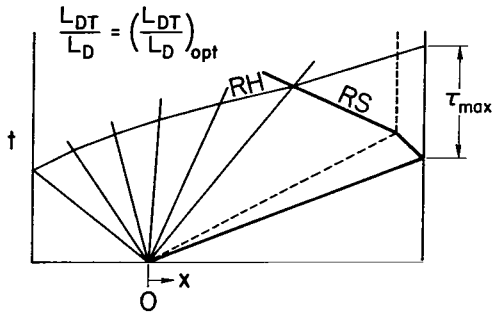

Sketch (a)

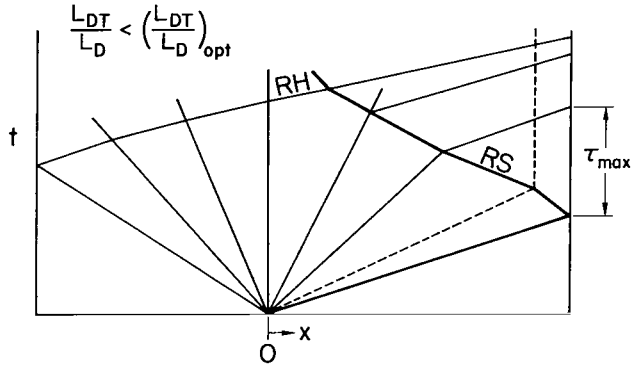

Sketch (b)

From sketch (a) it is seen that $(L_{DT}/L_D)_{opt}$ occurs when the reflected shock wave, the reflected expansion head, and the expansion tail all intersect at the same point on a distance-time diagram. When the component length ratio is less than the optimum value (sketch (b)), τ is limited by the disturbance generated from the interaction of the reflected shock wave and the driver gas expansion tail. Hence for a fixed driven tube length, increasing the driver length so that $(L_{DT}/L_D) < (L_{DT}/L_D)_{opt}$ requires more driver energy (larger volume) with no increase in the steady-state time, τ. For a fixed driver length (and energy), (L_{DT}/L_D) becomes less than $(L_{DT}/L_D)_{opt}$ when the driven tube length is too short. The result is that $\tau < \tau_{max}$ and the test-slug length is also reduced. Hence the situation depicted in sketch (a) is the optimum condition.

For component length ratios equal to or greater than the optimum value the reservoir steady-state time is limited by the arrival of the reflected expansion head from the driver. Increasing the component length ratio beyond the optimum value decreases τ until the reflected expansion head intersects the interface before the reflected shock wave, thus interfering with the tailoring process. Hence, for tailoring to occur the component length ratio must be less than a maximum value $(L_{DT}/L_D)_{max}$ (see sketch (c)). The allowable $(L_{DT}/L_D)_{max}$ therefore implies a minimum value, τ_{min}. The dependence of τ on the component length ratio is shown qualitatively in sketch (d) for fixed

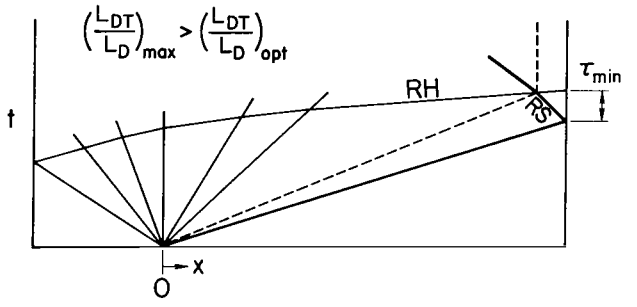

Sketch (c)

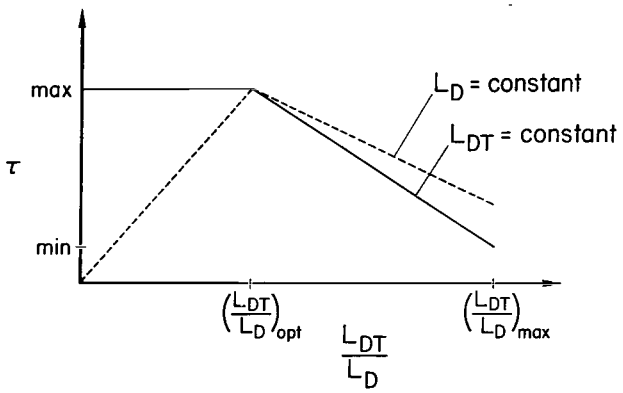

Sketch (d)

thermodynamic conditions in the driver and driven tube. It is seen that the curve for τ depends on which component length is allowed to vary. From the consideration of slopes on a distance-time diagram, relations for the variables above can be derived in terms of flow, wave, and sound speeds in the various regions, and the driver-gas specific heat ratio. These relations are derived in appendix B and are written in the following form:

(Note: $\gamma = \gamma_4$ in eqs. (8) through (15))

$$\left(\frac{L_{DT}}{L_D}\right)_{opt} = \frac{\left(\frac{\gamma + 1}{2} u_3 - a_4 + V_{RHe}\right)(u_3 + V_R)\left(1 - \frac{\gamma - 1}{2}\frac{u_3}{a_4}\right)^{-\frac{\gamma+1}{2(\gamma-1)}}}{(u_3 + V_{RHe})\left(1 + \frac{V_R}{V_{ST}}\right)a_4} \tag{8}$$

$$\left(\frac{L_{DT}}{L_D}\right)_{max} = \frac{2(u_3 + V_R)\left(1 - \frac{\gamma - 1}{2}\frac{u_3}{a_4}\right)^{-\frac{\gamma+1}{2(\gamma-1)}}}{\left(1 + \frac{V_R}{V_{ST}}\right)a_4} \tag{9}$$

$$\tau_{max} = L_D\left\{\left[\left(\frac{V_R}{a_5} - \frac{V_{RHe}}{a_6}\right)\left(\frac{1 + \frac{V_R}{V_{ST}}}{u_3 + V_R}\right) - \left(\frac{1 + \frac{V_R}{a_5}}{V_{ST}}\right)\right]\left(\frac{L_{DT}}{L_D}\right)_{opt} + \left(1 + \frac{V_{RHe}}{a_6}\right)\left[\frac{\left(1 - \frac{\gamma - 1}{2}\frac{u_3}{a_4}\right)^{-\frac{\gamma+1}{2(\gamma-1)}}}{a_4}\right]\right\} \tag{10}$$

$$\tau_{min} = L_D\left[\left(1 + \frac{V_R}{a_5}\right)\left(\frac{1 + \frac{V_R}{V_{ST}}}{u_3 + V_R} - \frac{1}{V_{ST}}\right)\right]\left(\frac{L_{DT}}{L_D}\right)_{max} \tag{11}$$

$$\tau = L_D \left\{ \left[\left(\frac{V_R}{a_5} - \frac{V_{RHe}}{a_6} \right) \left(\frac{1 + \frac{V_R}{V_{ST}}}{u_3 + V_R} \right) \right. \right.$$

$$\left. + \left(1 + \frac{V_{RHe}}{a_6} \right) \left(\frac{u_3 + V_{RHe}}{a_4 + \frac{3 - \gamma}{2} u_3 + V_{RHe}} \right) \left(\frac{1 + \frac{V_R}{V_{ST}}}{u_3 + V_R} \right) - \left(\frac{1 + \frac{V_R}{a_5}}{V_{ST}} \right) \right] \frac{L_{DT}}{L_D}$$

$$+ \left(1 + \frac{V_{RHe}}{a_6} \right) \left[\frac{2a_4 - (\gamma - 1)u_3}{a_4 + \frac{3 - \gamma}{2} u_3 + V_{RHe}} \right] \left. \left[\frac{\left(1 - \frac{\gamma - 1}{2} \frac{u_3}{a_4} \right)^{- \frac{\gamma+1}{2(\gamma-1)}}}{a_4} \right] \right\} \quad (12)$$

valid for

$$\left(\frac{L_{DT}}{L_D} \right)_{opt} < \frac{L_{DT}}{L_D} < \left(\frac{L_{DT}}{L_D} \right)_{max}$$

where

$$V_{RHe} = u_3 \left(\frac{1 + \frac{\gamma + 1}{\gamma - 1} \frac{p_5}{p_2}}{\frac{\gamma + 1}{\gamma - 1} + \frac{p_5}{p_2}} - 1 \right)^{-1} \quad (13)$$

$$a_6 = \left(a_4 - \frac{\gamma - 1}{2} u_3 \right) \left(\frac{p_5}{p_2} \frac{\frac{\gamma + 1}{\gamma - 1} + \frac{p_5}{p_2}}{1 + \frac{\gamma + 1}{\gamma - 1} \frac{p_5}{p_2}} \right)^{1/2} \quad (14)$$

and

$$a_4 = (\gamma R_4 T_4)^{1/2} \quad (15)$$

Equation (12) enables the determination of the available time τ for any component length ratio between the optimum and maximum values. Equations (8) through (12) are valid when the test gas is treated as a perfect gas as well as when real-gas effects are considered. The variables a_5, u_3, p_5/p_2, and V_R are found in the charts of references 6 through 12.

The length of the test-gas slug contained between the stationary interface and the driven tube end-wall for the tailored condition is determined from the relation

$$L_{TS} = \frac{\rho_1}{\rho_5} L_{DT}$$

or in terms of velocities

$$L_{TS} = \frac{(V_{ST} - u_2)V_R}{(V_R + u_2)V_{ST}} L_{DT} \qquad (16)$$

RESULTS AND DISCUSSION

Comparison of Perfect- and Real-Gas Calculations

The variation of tailored shock Mach number with driver temperature and initial loading pressure in the driven tube is shown in figure 2 for the several test gases considered. The effects of initial pressure are seen to be small. Comparisons with the perfect-gas strong-shock approximations illustrate a substantial deviation in tailored Mach numbers greater than $M_{ST} = 8$; for example, for $T_4 = 8000^\circ$ K, $p_1 = 0.001$ atm in air, the real-gas Mach number is 23.1 as compared to 19.4 for the perfect-gas value, an increase of 19 percent. In figure 2(d), real-gas effects in argon result in a lower M_{ST} than the perfect-gas value for 1000° K $< T_4 < 4000^\circ$ K. This behavior is due to the rapid onset of ionization in the test gas behind the reflected shock wave with increasing temperature. The relatively sudden transition to the ionized state reflects the existence of only sparsely populated excited electronic states that is characteristic of this gas (see ref. 10). The results for reflected shock pressures shown in reference 10 are consistent with present findings. It should be noted that in figure 2 the driver pressure p_4 is not arbitrary and must be determined from figure 3. However, since the effects of p_1 are small, then the effects of p_4 on the tailored shock Mach number are also small.

Figure 3 illustrates the effect of driver pressure and temperature on the initial loading pressure that is required in the driven tube to achieve interface tailoring. It is seen that p_1 is more sensitive to the driver conditions at lower driver temperatures. For CO_2 (fig. 3(c)), the curves for driver temperatures from 3000° to 6000° K lie close together while those for 4000° and 5000° K are seen to cross. Although not completely understood, this behavior is attributed to relatively large changes in chemical composition of the test gas with temperature in this interval and to the pressure dependence

of this change. For this range of driver temperatures the dissociation of CO_2 molecules is completed behind the incident shock wave and the further breakdown of the gas into C and O atoms is accomplished in substantial and varying amounts behind the reflected shock wave, as shown by the results of reference 9.

The test-gas reservoir or reflected shock enthalpy and pressure for tailored operation are shown as a function of driver temperature in figure 4. Again the driver pressure p_4 is not arbitrary and must be determined from figure 3. The enthalpy is in the dimensionless form h_5/RT_0 and the pressure is ratioed to the initial pressure p_1. Again the real-gas effects are obviously substantial. For air, with $T_4 = 8000^\circ$ K, $p_1 = 0.001$ atm, the reservoir enthalpy is 37 percent higher than the perfect-gas value and the reservoir pressure is 270 percent higher. This, of course, is a direct result of the real-gas tailoring Mach number being greater than the perfect-gas value. When the reservoir enthalpy is a specified quantity, say for design purposes $h_5/RT_0 = 700$ in air, then if the real-gas effects are considered the driver temperature required will be less than the required perfect-gas value, in this case by 25 percent. Similar results are observed for N_2 and CO_2. With argon, however, the advantageous effects of real-gas properties are less pronounced. In fact, for $h_5/RT_0 < 500$ real-gas effects are disadvantageous, reflecting again the presence of substantial amounts of ionization in the test gas at relatively low values of T_4.

The optimum and allowable maximum component length ratios are shown in figure 5 as a function of driver temperature with p_1 as a parameter. The real-gas length ratios are greater by as much as a factor of 2 and a surprisingly large influence of test-gas chemistry can be seen for CO_2 and argon, at the T_4 values noted earlier in figures 2 and 3. From comparison with the perfect-gas values it is noted that, for a <u>given driven tube length</u>, considering real-gas effects enables the use of a shorter driver; therefore, less total driver energy is required for a specified driver pressure and temperature. Conversely, for a <u>given driver length</u> the optimum driven tube length must be substantially greater than predicted by a perfect-gas analysis to achieve a maximum real-gas, steady-state reservoir time. The intermediate situations where L_{DT}/L_D is less than optimum should be avoided since they have been shown earlier to have adverse effects on steady-state times and driver energy requirements (see sketches (b) and (d)).

Figure 6 illustrates the effects of driver temperature and initial pressure p_1 on the steady-state time parameter $a_1\tau/L_D$. The parameter, and therefore the available steady-state time τ, decreases with increasing temperature and depends slightly on the initial pressure in the driven tube. For a given driver temperature and initial pressure, the consideration of real-gas effects yields a value for the parameter less than the perfect-gas value. The deviations are less pronounced for the optimum values of L_{DT}/L_D than for the maximum values. For example, at $T_4 = 8000^\circ$ K, $p_1 = 0.001$ atm from figure 6(a) the deviation in the parameter is only 8 percent for the optimum case but is 40 percent for the maximum. This is so for two reasons: First, in the optimum case the controlling feature is the velocity of the primary expansion tail. While this disturbance moves much faster relative to the main shock wave in the real-gas flow than in the perfect gas, the added driven tube

length required for real-gas optimization is compensatory and τ is not greatly different. Second, in the case of maximum L_{DT}/L_D the length of the test-gas slug (see eq. (16)) is dominant and is sufficiently reduced in the real gas that even the greater driven tube length does not overcome the difference, and τ is substantially less. In summary, if driver length is fixed, the increase in driven tube length to meet the real-gas optimum condition largely compensates for the time reduction (per foot of tube) due to real-gas effects. If, however, the driven tube is fixed and the driver is shortened to minimize energy requirements for real-gas operation, then the combined results of figures 5(a) and 6(a) reveal the steady-state time $\tau_{opt}{}_{real} \approx 0.40\ \tau_{opt}{}_{perfect}$. For a long driver, when L_{DT}/L_D is less than $(L_{DT}/L_D)_{opt}$ time does not increase so long as the driven tube length is fixed, as was indicated in the Analysis section. This last condition might not be restrictive if the relatively slow change of pressure in the primary expansion tail can be tolerated (see sketch (b)).

Use of Charts

The use of the charts will be illustrated by the following examples. The first example is to determine the conditions required for tailored operation of a shock tunnel for a given set of driver conditions, say $T_4 = 4000^\circ$ K and $p_4 = 400$ atm, in a helium-air gas combination. From figures 2(a) and 3(a) the required shock Mach number is $M_{ST} = 14.7$, and the initial driven tube loading pressure $p_1 = 0.10$ atm. The reservoir or reflected shock enthalpy and pressure are found to be $h_5/RT_o = 365$ or $h_5 = 28.72 \times 10^6$ joules/kg, and $p_5/p_1 = 3350$ or $p_5 = 335$ atm, from figure 4(a). These values as well as the remaining reservoir properties and the conditions downstream of the incident shock wave can be found from the charts of references 6, 7, and 12. Pertinent values for this example are $u_2 = 4.62$ mm/μsec, $V_R = 0.843$ mm/μsec, and $a_5 = 2.24$ mm/μsec. From equations (8) through (11) or from figures 5(a) and 6(a), $(L_{DT}/L_D)_{opt} = 2.5$, $(L_{DT}/L_D)_{max} = 7.3$, $(a_1\tau/L_D)_{max} = 0.152$, and $(a_1\tau/L_D)_{min} = 0.062$. Therefore for a driver length, L_D, of 3.0 m, $(L_{DT})_{opt} = 7.5$ m, $(L_{DT})_{max} = 21.9$ m, $\tau_{max} = 1.314$ msec, and $\tau_{min} = 0.536$ msec. The length of the reservoir test slug is found from equation (16); $(L_{TS})_{opt} = 0.111$ m, $(L_{TS})_{max} = 0.328$ m.

The second example is to determine the conditions required for tailored operation of a shock tunnel for a He-CO_2 gas combination for a given reservoir enthalpy and pressure, say $h_5 = 28.30 \times 10^6$ joules/kg and $p_5 = 98$ atm. From figure 4(c) the driver temperature is $T_4 = 3000^\circ$ K and the loading pressure is $p_1 = 0.01$ atm, found by a trial and error selection of p_1 in the figure. From figures 2(a) and 3(a) the required shock Mach number is $M_{ST} = 19.0$ and the required driver pressure is $p_4 = 140$ atm. The same procedure as in the first example is used to determine the remaining reservoir properties, conditions behind the incident shock wave, component lengths and steady-state times τ.

CONCLUDING REMARKS

An analytical and numerical study has been made of shock tube performance in the tailored-interface mode of operation, with primary emphasis on the influence of equilibrium real-gas effects in the test medium. The effects of viscosity, energy radiation, and nonideal wave interactions have not been considered in this study, and to this extent the specific results will be at variance with experimental findings.

The perfect-gas relations for the tailoring requirement are summarized and a computer method is presented that extends the perfect-gas results to include equilibrium real-gas effects in the test gas. Equations are derived for determining the time during which the reservoir properties remain constant. Charts are presented that facilitate the determination of the flow and thermodynamic properties for tailored operation for a constant-area shock tube employing a helium driver and air, CO_2, N_2, or argon as test gases. Driver conditions are varied from 300° K $\leq T_4 \leq 10{,}000^\circ$ K and 10 atm $\leq p_4 \leq$ 1,500 atm.

The results deviate substantially from the perfect-gas results when real-gas effects are considered, especially for tailored Mach numbers greater than 8. With respect to driver length and energy requirements these deviations are very favorable. For a given driver pressure and temperature the real-gas tailored Mach number, and hence the reservoir enthalpy, is considerably higher than the perfect-gas value. This result is important in an experiment (e.g., heat transfer) for which the reservoir enthalpy level is a given quantity. Considering real-gas effects can reduce the driver temperature requirements by as much as 30-50 percent, with a corresponding reduction in driver energy requirements. In addition to the reduction in driver temperature requirements for a given reservoir enthalpy, a further reduction in total driver energy is apparent from the fact that a shorter driver is required for a given driven-tube length.

It is shown that a maximum steady-state time, τ, exists and corresponds to the optimum component length ratio. A minimum steady-state time also exists, if tailoring is to be achieved, and corresponds to the maximum allowable component length ratio. The time, τ, during which the reservoir properties remain constant is reduced from the ideal-gas value. The consideration of real-gas effects is a necessity when conditions are determined for tailored-interface operation at Mach numbers above 8 and driver gas temperatures in excess of 1000° K.

Ames Research Center
National Aeronautics and Space Administration
Moffett Field, Calif., March 18, 1966

APPENDIX A

COMPUTATIONAL PROCEDURE AND ITERATION METHODS

An IBM 7094 Fortran II program incorporates as input information the following thermodynamic properties in the driver and driven tube: p_1, T_1, γ_1, R_1, p_4, T_4, γ_4, and R_4. The driver gas speed of sound and limiting velocity are calculated from

$$a_4 = (\gamma_4 R_4 T_4)^{1/2} \tag{A1}$$

and

$$u_L = a_4\left(\frac{2}{\gamma_4 - 1}\right) \tag{A2}$$

Equation (A2) is necessary in the iteration method for matching pressure and velocity across the incident interface.

INITIAL MOVING SHOCK WAVE

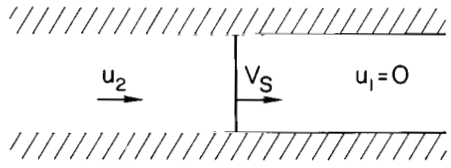

Sketch (e)

The flow geometry is illustrated in sketch (e). A Galilean transformation is used to rewrite equations (6) as follows:

$$\left.\begin{aligned} p_2 &= p_1 + \rho_1 V_S^2\left(1 - \frac{\rho_1}{\rho_2}\right) \\ h_2 &= h_1 + \frac{V_S^2}{2}\left[1 - \left(\frac{\rho_1}{\rho_2}\right)^2\right] \\ \frac{\rho_1}{\rho_2} &= 1 - \frac{u_2}{V_S} \\ \rho_2 &= \rho_2(p_2, h_2) \end{aligned}\right\} \tag{A3}$$

The choice of an initial value of u_2/V_S, for example, $u_2/V_S = 1$, leads to first approximations for p_2 and h_2. From thermodynamic tables a ρ_2 and thus an improved value for u_2/V_S is found. The cycle is repeated until successive values of u_2/V_S differ by a negligible amount.

ITERATION FOR EQUAL PRESSURES ACROSS INTERFACE

The driver gas is expanded unsteadily from stagnation conditions to a pressure p_3. From equation (7)

$$p_3 = p_4\left(1 - \frac{\gamma_4 - 1}{2}\frac{u_3}{a_4}\right)^{\frac{2\gamma_4}{\gamma_4 - 1}} \tag{A4}$$

where p_4 is given and a_4 is known from equation (A2). The iteration consists of initially choosing two values for $u_2 = u_3$ and comparing the resulting p_3 from equation (A4) with p_2 from the initial moving shock relations (A3). The method is illustrated in sketch (f). The curve for p_3

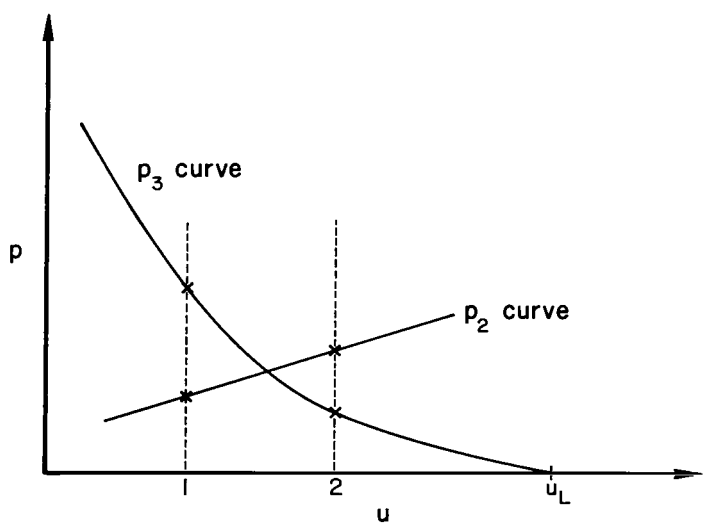

Sketch (f)

is arbitrarily fitted with a parabola through the two chosen values for u_2 and the limiting velocity, u_L. The p_2 curve is approximated arbitrarily with a straight line. The intersection of the two curves defines a new estimate for the velocity u_2 which is used to compute new p_2 and p_3. The iteration proceeds in this manner until the following criterion for convergence is satisfied:

$$\left|\frac{p_2 - p_3}{p_2}\right| < 0.00005$$

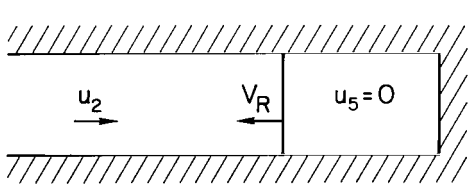

Sketch (g)

REFLECTED SHOCK WAVE

The flow geometry is illustrated in sketch (g). Equations (6) of the text, after a Galilean transformation, are rewritten in the form

$$\left.\begin{aligned} p_5 &= p_2 + \rho_2(V_R + u_2)^2\left(1 - \frac{\rho_2}{\rho_5}\right) \\ h_5 &= h_2 + \frac{1}{2}(p_5 - p_2)\left(\frac{1}{\rho_2} + \frac{1}{\rho_5}\right) \\ \frac{\rho_5}{\rho_2} &= \left(1 + \frac{u_2}{V_R}\right) \\ \rho_5 &= \rho_5(p_5, h_5) \end{aligned}\right\} \qquad (A5)$$

where the properties in region 2 are known. The choice of an initial value of u_2/V_R (e.g., $u_2/V_R = 1$) leads to first approximations for p_5 and h_5. From the thermodynamic tables a ρ_5 and thus an improved value for u_2/V_R is found. The process is repeated until successive values of u_2/V_R differ by a negligible amount.

REFLECTION AND REFRACTION OF THE REFLECTED SHOCK WAVE AT THE INTERFACE

The flow geometry is illustrated in sketch (h). For the refracted shock wave, which transmits into the driver gas (considered to be a perfect gas), the shock equations become

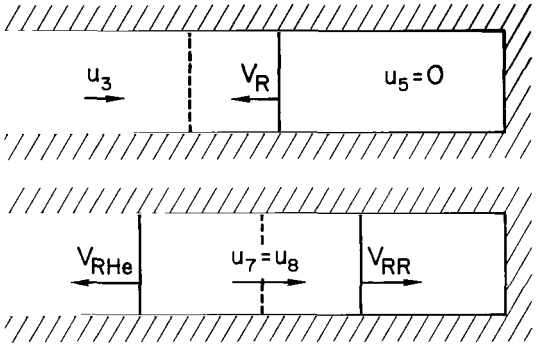

Sketch (h)

$$p_7 = p_3 + \rho_3(u_3 + V_{RHe})^2\left(1 - \frac{\rho_3}{\rho_7}\right) \qquad (A6a)$$

$$\frac{\rho_7}{\rho_3} = \frac{u_3 + V_{RHe}}{u_7 + V_{RHe}} \qquad (A6b)$$

and

$$\frac{p_7}{p_3} = \frac{\frac{\gamma_4 + 1}{\gamma_4 - 1}\frac{\rho_7}{\rho_3} - 1}{\frac{\gamma_4 + 1}{\gamma_4 - 1} - \frac{\rho_7}{\rho_3}} \tag{A6c}$$

The reflected wave from the interface can be a shock wave, a Mach wave, or an expansion wave, depending upon the initial loading pressure in the driven tube. When it is a shock wave, the governing equations are

$$\left.\begin{aligned} p_8 &= p_5 + \rho_5 V_{RR}^2\left(1 - \frac{\rho_5}{\rho_8}\right) \\ h_8 &= h_5 + \frac{V_{RR}^2}{2}\left[1 - \left(\frac{\rho_5}{\rho_8}\right)^2\right] \\ \frac{\rho_5}{\rho_8} &= 1 - \frac{u_8}{V_{RR}} \\ \rho_8 &= \rho_8(p_8, h_8) \end{aligned}\right\} \tag{A7}$$

The wave reflected from the interface will be a shock when $u_7 = u_8 > 0$. The boundary conditions are $p_7 = p_8$ and $u_7 = u_8$. The procedure for solving equations (A6) and (A7) is as follows:

(1) Let $u_8 = 0$, as a first guess.

(2) Assume a ρ_7/ρ_3 and calculate a p_7/p_3 from equation (A6c).

(3) Calculate V_{RHe} from equation (A6a).

(4) Calculate ρ_7/ρ_3 from equation (A6b) and repeat steps (2) to (4) until the successive values of ρ_7/ρ_3 differ by a negligible amount.

(5) If the input p_1 is sufficiently small, the resulting p_7 is greater than p_5. The computer now solves equations (A7) for the guessed value u_8 and compares p_8 with p_7. If $p_7 \neq p_8$ a new estimate for u_8 is made.

(6) Using the new u_8, repeat steps (2) to (5) until successive values of u_8 differ by a negligible amount, thus determining the conditions in regions (7) and (8). The result is that $p_7 = p_8$, $u_7 = u_8 > 0$, and $p_8/p_5 > 1$.

DETERMINING THE INITIAL DRIVEN TUBE LOADING PRESSURE FOR TAILORED OPERATION

For a given set of driver conditions, the input p_1 is selected sufficiently small that a shock wave is reflected from the interface as illustrated in sketch (h). New values of p_1 are successively computed from

$$p_{1_{new}} = \frac{p_8}{p_5} p_1 \tag{A8}$$

and the entire process beginning with the incident shock wave is repeated until the following criterion is established:

$$1.000 < \frac{p_8}{p_5} \leq 1.005$$

As $p_8/p_5 \rightarrow 1$, $u_7 = u_8 \rightarrow 0$ and the interface is considered to be tailored.

APPENDIX B

DERIVATION OF COMPONENT LENGTH AND RESERVOIR STEADY-STATE TIME RELATIONS

GENERAL EQUATIONS

The equations are derived in terms of wave and flow velocities and the driver specific heat ratio. Variables used in the derivations are defined in the distance-time diagram below.

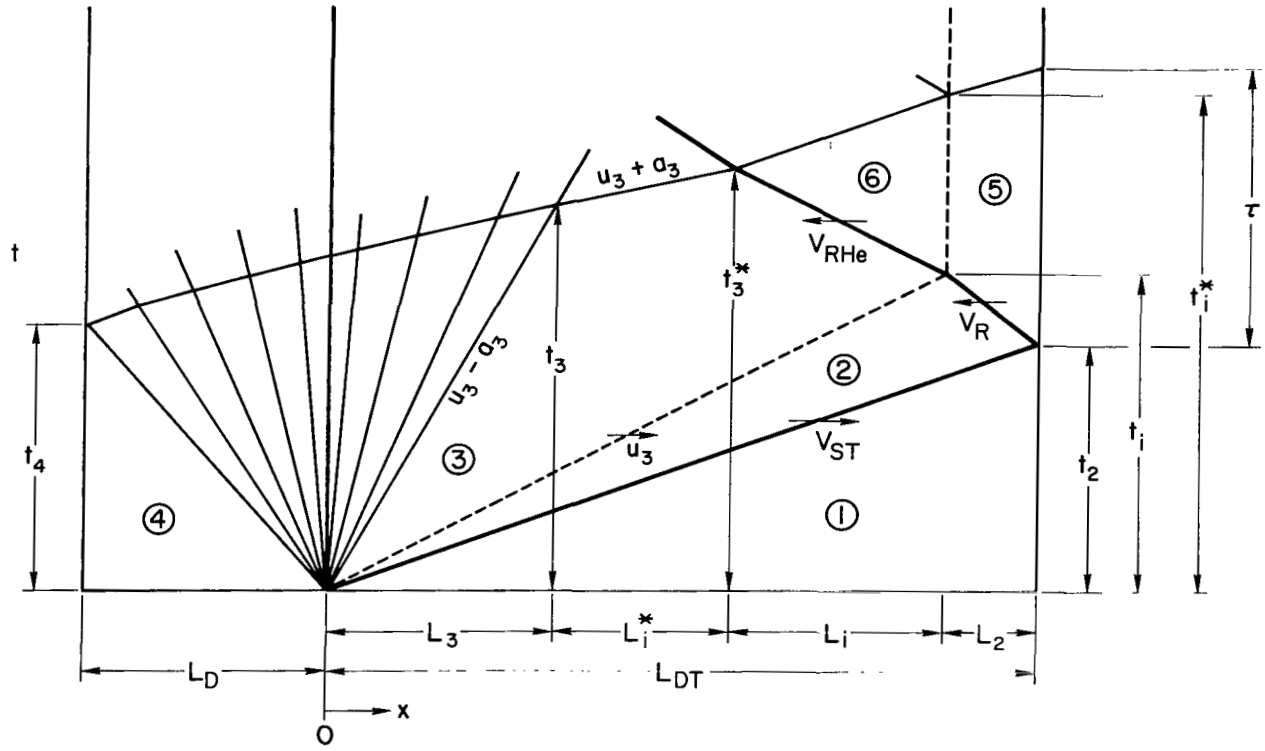

Sketch (i)

The time for which the reflected expansion head from the driver wall and the expansion tail intersect, t_3, is found by the method of reference 15. For a perfect gas it can be shown that

(Note: $\gamma = \gamma_4$ in the following equations)

$$\frac{(at^2)_3}{(at^2)_4} = \left(\frac{a_4}{a_3}\right)^{\frac{2}{\gamma-1}}$$

which, after rearrangement, becomes

$$t_3 = t_4\left(\frac{a_4}{a_3}\right)^{\frac{\gamma+1}{2(\gamma-1)}} \tag{B1}$$

The driver length is

$$L_D = a_4 t_4$$

or

$$t_4 = \frac{L_D}{a_4} \tag{B2}$$

The equation for the isentropic unsteady expansion of a perfect gas from stagnation conditions can be written as

$$\frac{a_4}{a_3} = \left(1 - \frac{\gamma - 1}{2}\frac{u_3}{a_4}\right)^{-1} \tag{B3}$$

Combining equations (B1), (B2), and (B3) results in the intersection time

$$t_3 = \frac{L_D}{a_4}\left(1 - \frac{\gamma - 1}{2}\frac{u_3}{a_4}\right)^{-\frac{\gamma+1}{2(\gamma-1)}} \tag{B4}$$

From the sketch the following equations can be written:

$$L_{DT} = L_3 + L_i^* + L_i + L_2 \tag{B5}$$

$$L_3 = (u_3 - a_3)t_3 \tag{B6}$$

$$L_i = V_{RHe}(t_3^* - t_i) = a_6(t_i^* - t_3^*) \tag{B7}$$

$$L_i^* = (u_3 + a_3)(t_3^* - t_3) \tag{B8}$$

$$L_2 = V_R(t_i - t_2) = V_R t_i - \frac{V_R}{V_{ST}} L_{DT}$$

$$= a_5\left(\tau + \frac{L_{DT}}{V_{ST}} - t_i^*\right) \tag{B9}$$

where $L_{DT}/V_{ST} = t_2$

$$L_3 + L_i^* + L_i = u_3 t_i \tag{B10}$$

From equations (B5), (B9), and (B10)

$$t_i = L_{DT}\left(\frac{1 + \frac{V_R}{V_{ST}}}{u_3 + V_R}\right) \tag{B11}$$

Equating (B6), (B7), and (B8) to equation (B10) yields

$$(u_3 - a_3)t_3 + V_{RHe}t_3^* - V_{RHe}t_i + (u_3 + a_3)t_3^* - (u_3 + a_3)t_3 = u_3 t_i$$

From equation (B3), the above equation can be rearranged as follows

$$t_3^* = \left(\frac{u_3 + V_{RHe}}{a_4 + \frac{3 - \gamma}{2} u_3 + V_{RHe}}\right)t_i + \left[\frac{2a_4 - (\gamma - 1)u_3}{a_4 + \frac{3 - \gamma}{2} u_3 + V_{RHe}} - 1\right] t_3 \tag{B12}$$

Combining equations (B4), (B11), and (B12) gives

$$t_3^* = \left(\frac{u_3 + V_{RHe}}{a_4 + \frac{3 - \gamma}{2} u_3 + V_{RHe}}\right)\left(\frac{1 + \frac{V_R}{V_{ST}}}{u_3 + V_R}\right)L_{DT}$$

$$+ \left[\frac{2a_4 - (\gamma - 1)u_3}{a_4 + \frac{3 - \gamma}{2} u_3 + V_{RHe}}\right]\left[\frac{\left(1 - \frac{\gamma - 1}{2}\frac{u_3}{a_4}\right)^{-\frac{\gamma+1}{2(\gamma-1)}}}{a_4} - 1\right] L_D \tag{B13}$$

The time for which the reflected expansion head and the tailored-interface interact is found by solving equation (B7) for t_i^*,

$$t_i^* = \left(1 + \frac{V_{RHe}}{a_6}\right) t_3^* - \frac{V_{RHe}}{a_6} t_i \tag{B14}$$

The time, τ, during which the reservoir thermodynamic properties remain constant is the interval between the arrival of the reflected expansion head and the incident shock wave in the reservoir. From equation (B9),

$$\tau = \frac{V_R}{a_5} t_i + t_i^* - \left(\frac{1 + \frac{V_R}{a_5}}{V_{ST}}\right) L_{DT} \tag{B15}$$

When equations (B11), (B14), and (B15) are combined, τ becomes

$$\tau = \left[\left(\frac{V_R}{a_5} - \frac{V_{RHe}}{a_6}\right)\left(\frac{1 + \frac{V_R}{V_{ST}}}{u_3 + V_R}\right) - \left(\frac{1 + \frac{V_R}{a_5}}{V_{ST}}\right)\right] L_{DT} + \left(1 + \frac{V_{RHe}}{a_6}\right) t_3^* \tag{B16}$$

The general equation for the time τ in terms of known driver and driven tube lengths and the various wave, flow, and sound speeds is found by combining equations (B13) and (B16),

$$\tau = L_D \left\{ \left[\left(\frac{V_R}{a_5} - \frac{V_{RHe}}{a_6}\right)\left(\frac{1 + \frac{V_R}{V_{ST}}}{u_3 + V_R}\right) + \left(1 + \frac{V_{RHe}}{a_6}\right)\left(\frac{u_3 + V_{RHe}}{a_4 + \frac{3 - \gamma}{2} u_3 + V_{RHe}}\right)\left(\frac{1 + \frac{V_R}{V_{ST}}}{u_3 + V_R}\right) \right.\right.$$

$$\left.\left. - \left(\frac{1 + \frac{V_R}{a_5}}{V_{ST}}\right)\right] \frac{L_{DT}}{L_D} + \left(1 + \frac{V_{RHe}}{a_6}\right)\left[\frac{2a_4 - (\gamma - 1)u_3}{a_4 + \frac{3 - \gamma}{2} u_3 + V_{RHe}}\right]\left[\frac{\left(1 - \frac{\gamma - 1}{2}\frac{u_3}{a_4}\right)^{-\frac{\gamma+1}{2(\gamma-1)}}}{a_4}\right] \right\} \tag{B17}$$

Equation (B17) holds for any L_{DT}/L_D such that $L_i^* > 0$ and $L_i > 0$. To evaluate equation (B17), a_6 and V_{RHe} must be calculated from the Rankine-Hugoniot relations. From the transfer of velocity coordinates in sketch (j), the ideal Rankine-Hugoniot relation is used to calculate the reflected shock velocity in the driver gas, V_{RHe}.

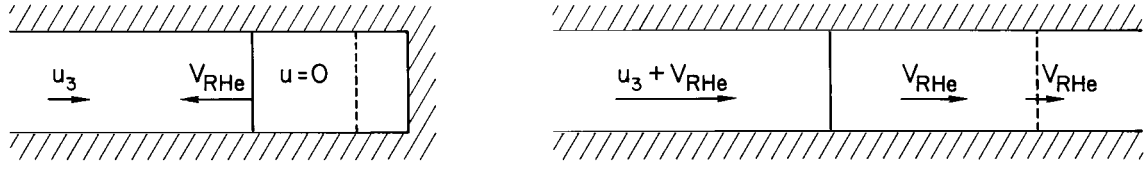

Sketch (j)

$$\frac{u_2}{u_5} = \frac{u_3 + V_{RHe}}{V_{RHe}} = \frac{1 + \frac{\gamma + 1}{\gamma - 1}\frac{p_5}{p_2}}{\frac{\gamma + 1}{\gamma - 1} + \frac{p_5}{p_2}}$$

Solving for V_{RHe},

$$V_{RHe} = u_3 \left(\frac{1 + \frac{\gamma + 1}{\gamma - 1} \frac{p_5}{p_2}}{\frac{\gamma + 1}{\gamma - 1} + \frac{p_5}{p_2}} - 1 \right)^{-1} \tag{B18}$$

The speed-of-sound ratio across the reflected shock in the driver gas is

$$\frac{a_6}{a_3} = \left(\frac{p_5}{p_2} \frac{\frac{\gamma + 1}{\gamma - 1} + \frac{p_5}{p_2}}{1 + \frac{\gamma + 1}{\gamma - 1} \frac{p_5}{p_2}} \right)^{1/2} \tag{B19}$$

Combining equations (B3) and (B19) yields

$$a_6 = \left(a_4 - \frac{\gamma - 1}{2} u_3 \right) \left(\frac{p_5}{p_2} \frac{\frac{\gamma + 1}{\gamma - 1} + \frac{p_5}{p_2}}{1 + \frac{\gamma + 1}{\gamma - 1} \frac{p_5}{p_2}} \right)^{1/2} \tag{B20}$$

where $a_4 (\gamma R T_4)^{1/2}$. The pressure ratio

$$\frac{p_5}{p_2} = \frac{p_5}{p_1} \frac{p_1}{p_2}$$

where p_5/p_1, p_1/p_2, and the remaining quantities V_{ST}, V_R, u_3, a_5 can be found from the charts in the references.

SPECIAL CASE EQUATIONS

Optimal Relations

Maximum time τ can be achieved when the reflected shock wave, reflected expansion head, and expansion tail intersect at the same point. From sketch (i) τ_{max} and thus $L_{DT}/L_D|_{opt}$ occur when $t_3^* = t_3$, $L_i^* = 0$. From equations (B4) and (B13)

$$t_3^* = t_3 = \frac{L_D}{a_4} \left(1 - \frac{\gamma - 1}{2} \frac{u_3}{a_4} \right)^{-\frac{\gamma+1}{2(\gamma-1)}} = \left(\frac{u_3 + V_{RHe}}{a_4 + \frac{3 - \gamma}{2} u_3 + V_{RHe}} \right) \left(\frac{1 + \frac{V_R}{V_{ST}}}{u_3 + V_R} \right) L_{DT}$$

$$+ \left[\frac{2a_4 - (\gamma - 1)u_3}{a_4 + \frac{3 - \gamma}{2} u_3 + V_{RHe}} \right] \left[\frac{\left(1 - \frac{\gamma - 1}{2} \frac{u_3}{a_4} \right)^{-\frac{\gamma+1}{2(\gamma-1)}}}{a_4} \right] L_D$$

which when rearranged yields the optimum component length ratio

$$\left.\frac{L_{DT}}{L_D}\right|_{opt} = \frac{\left(\frac{\gamma+1}{2}u_3 - a_4 + V_{RHe}\right)(u_3 + V_R)\left(1 - \frac{\gamma-1}{2}\frac{u_3}{a_4}\right)^{-\frac{\gamma+1}{2(\gamma-1)}}}{(u_3 + V_{RHe})\left(1 + \frac{V_R}{V_{ST}}\right)a_4} \tag{B21}$$

From equations (B4) and (B16) with $t_3^* = t_3$, the maximum time τ becomes

$$\tau_{max} = L_D\left\{\left[\left(\frac{V_R}{a_5} - \frac{V_{RHe}}{a_6}\right)\left(\frac{1 + \frac{V_R}{V_{ST}}}{u_3 + V_R}\right) - \left(\frac{1 + \frac{V_R}{a_5}}{V_{ST}}\right)\right]\left.\frac{L_{DT}}{L_D}\right|_{opt} + \left(1 + \frac{V_{RHe}}{a_6}\right)\left[\frac{\left(1 - \frac{\gamma-1}{2}\frac{u_3}{a_4}\right)^{-\frac{\gamma+1}{2(\gamma-1)}}}{a_4}\right]\right\} \tag{B22}$$

To evaluate equation (B22) one must assume a driver length.

Minimal Tailoring Relations

An upper limit on the component length ratio, $L_{DT}/L_{D_{max}}$, is imposed since the reflected shock wave must interact with the interface prior to the reflected expansion head if tailoring is to occur. From sketch (i), the limit results when $t_3^* = t_i^* = t_i$, $L_i = 0$. From equations (B11) and (B13) the maximum allowable component length ratio becomes

$$\left.\frac{L_{DT}}{L_D}\right|_{max} = \frac{2(u_3 + V_R)\left(1 - \frac{\gamma-1}{2}\frac{u_3}{a_4}\right)^{-\frac{\gamma+1}{2(\gamma-1)}}}{\left(1 + \frac{V_R}{V_{ST}}\right)a_4} \tag{B23}$$

From equations (B11) and (B16) with $t_3^* = t_i$, the minimum time τ becomes

$$\tau_{min} = L_D\left[\left(1 + \frac{V_R}{a_5}\right)\left(\frac{1 + \frac{V_R}{V_{ST}}}{u_3 + V_R} - \frac{1}{V_{ST}}\right)\right]\left.\frac{L_{DT}}{L_D}\right|_{max} \tag{B24}$$

Again one must assume a driver length.

REFERENCES

1. Cunningham, Bernard E.; and Kraus, Samuel: A 1-Foot Hypervelocity Shock Tunnel in Which High-Enthalpy, Real-Gas Air Flows Can be Generated With Flow Times of About 180 Milliseconds. NASA TN D-1428, 1962.

2. Loubsky, William J.; Hiers, Robert S.; and Stewart, David A.: Performance of a Combustion Driven Shock Tunnel With Application to the Tailored-Interface Operating Conditions. Presented at Third Conf. on Performance of High-Temperature Sys., Pasadena, Calif., Dec. 1964, 26 p.

3. Hertzberg, A.; Smith, W. E.; Glick, H. S.; and Square, W.: Modifications of the Shock Tube for the Generation of Hypersonic Flow. AEDC-TN-55-15, Arnold Engr. Dev. Ctr., March 1955.

4. Ford, C. A.; and Glass, I. I.: An Experimental Study of Shock-Wave Refraction. UTIA Rep. 29, Univ. of Toronto, Sept. 1954.

5. Flagg, R. F.: Detailed Analysis of Shock Tube Tailored Conditions. RAD-TM-63-64, Avco Corp., Sept. 1963.

6. Feldman, Saul: Hypersonic Gas Dynamic Charts for Equilibrium Air. Res. Rep. 40, Avco Everett, Jan. 1957.

7. Laird, J. D.; and Heron, K.: Shock Tube Gas Dynamic Charts. Part 1: Equilibrium Argon-Free Air From 3,000 to 40,000° K. RAD-TM-64-12, Avco Corp., April 1964.

8. Lewis, Clark H.; and Burgess, E. G., III: Charts of Normal Shock Wave Properties in Imperfect Nitrogen. AEDC-TDR-64-104, Aro, Inc., May 1964.

9. Simcox, Craig D.; and Peterson, Victor L.: Charts for Equilibrium and Frozen Flows Across Plane Shock Waves in Carbon Dioxide. NASA SP-3018, 1965.

10. Ahtye, Warren F.: A Critical Evaluation of Methods for Calculating Transport Coefficients of Partially and Fully Ionized Gases. NASA TN D-2611, 1965.

11. Huseby, O. A.: Aerothermodynamic Properties of High Temperature Argon. D2-11238, Boeing Co., 1962.

12. Moeckel, W. E.; and Weston, Kenneth C.: Composition and Thermodynamic Properties of Air in Chemical Equilibrium. NACA TN 4265, 1958.

13. Bailey, Harry E.: Equilibrium Thermodynamic Properties of Carbon Dioxide. NASA SP-3014, 1965.

14. Lick, Wilbert J.; and Emmons, Howard W.: Thermodynamic Properties of Helium to 50,000° K. Harvard Univ. Press, Cambridge, 1962.

15. Grose, William L.; and Trimpi, Robert L.: Charts for the Analysis of Isentropic One-Dimensional Unsteady Expansions in Equilibrium Real Air With Particular Reference to Shock-Initiated Flows. NASA TR R-167, 1963.

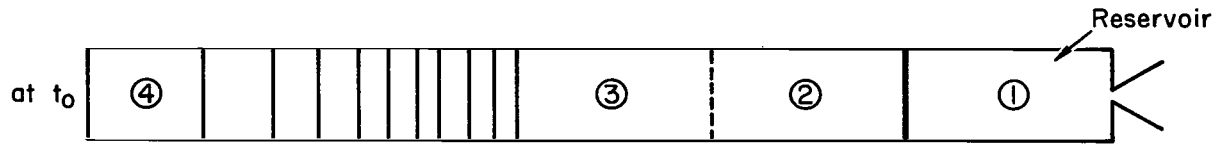

(a) Schematic diagram.

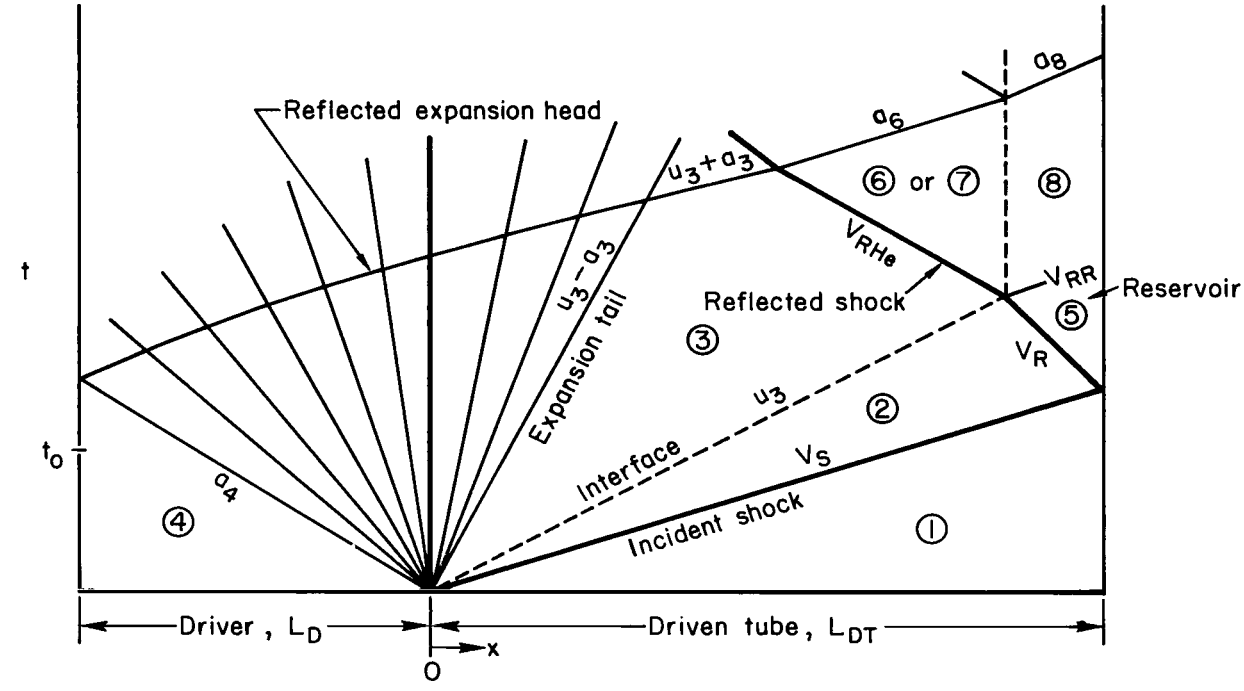

(b) Distance-time diagram.

Figure 1.- Schematic and distance-time diagrams for a constant area shock tube.

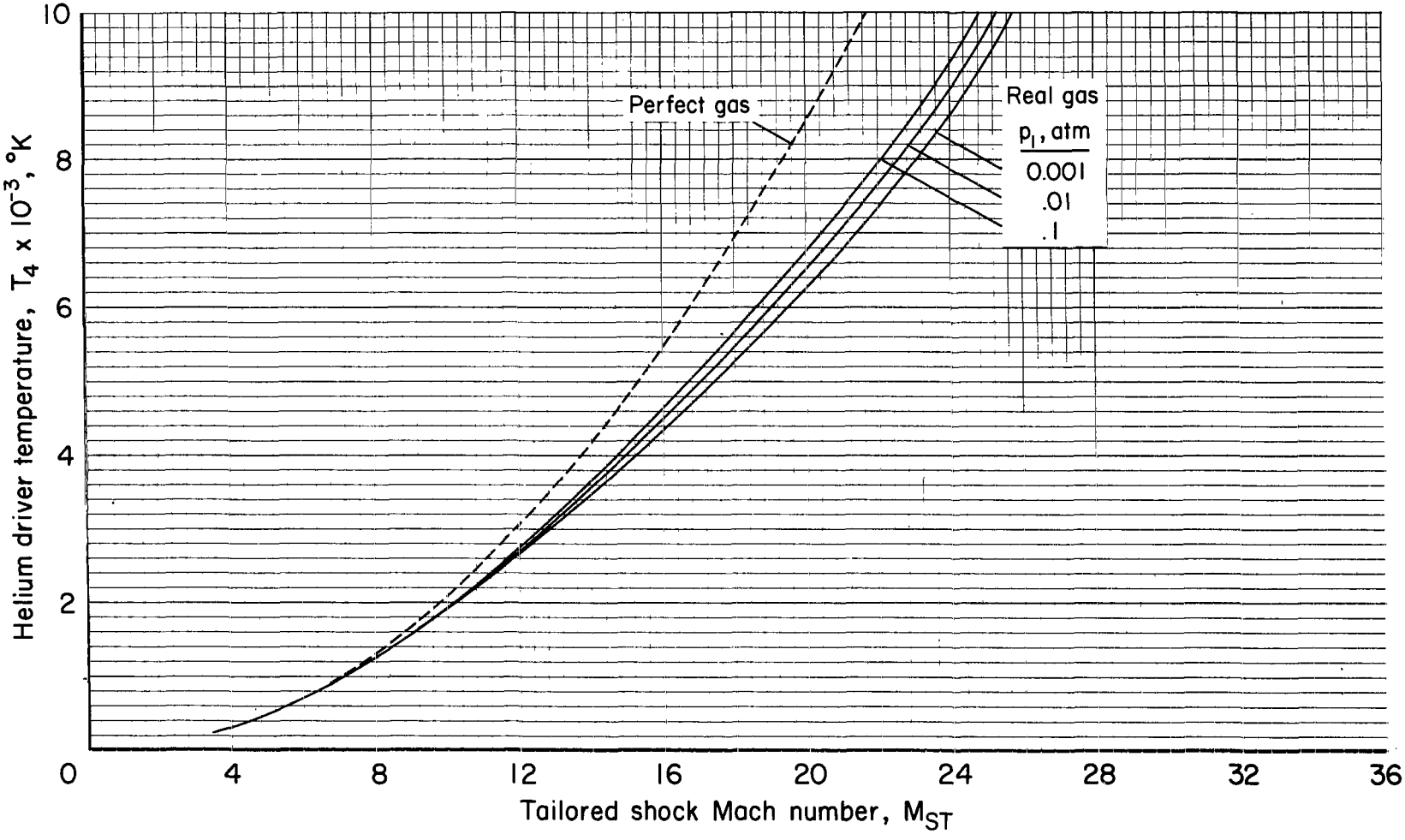

(a) Air.

Figure 2.- Driver-gas temperature required for a tailored shock wave (P_4 not arbitrary).

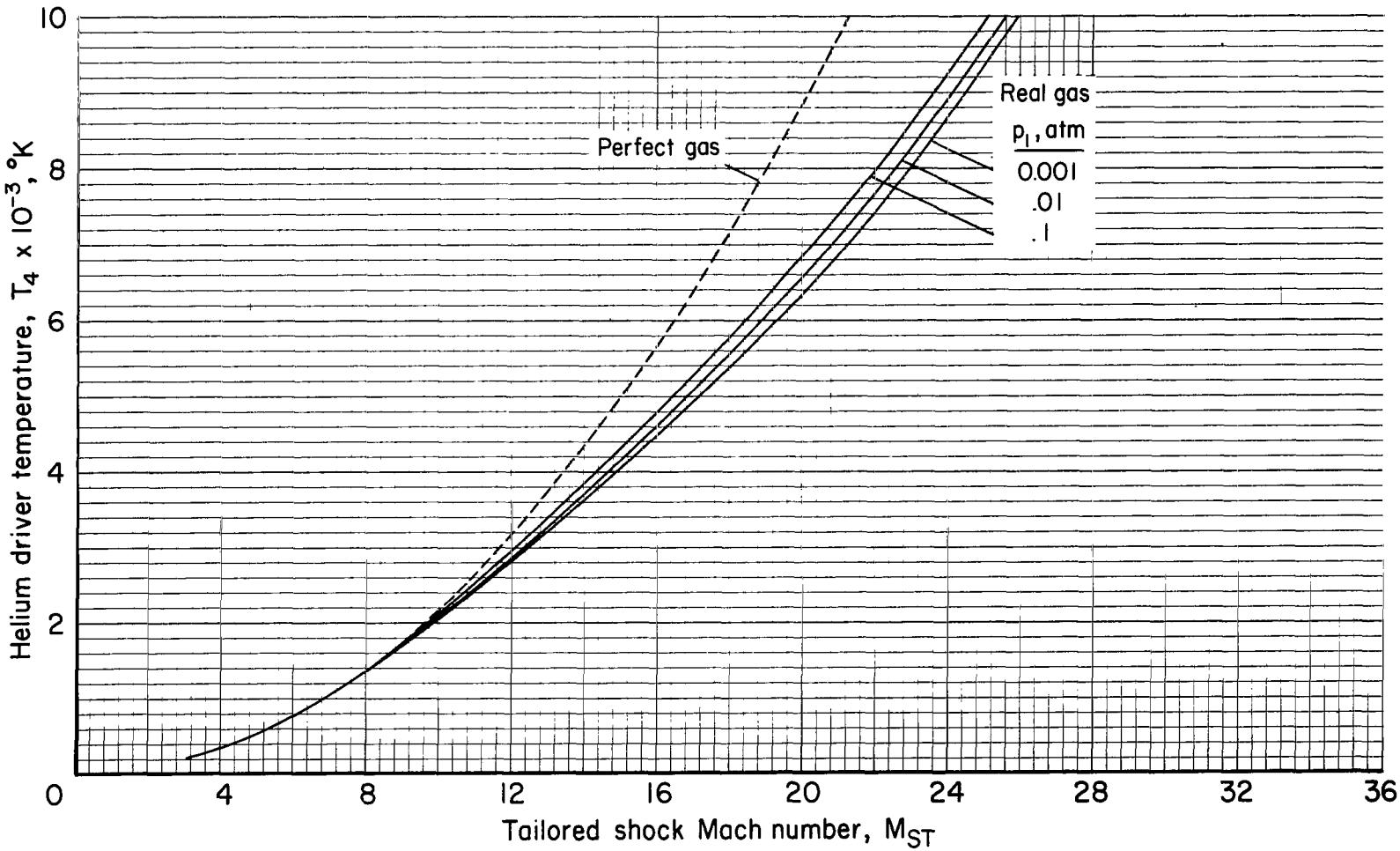

(b) Nitrogen.

Figure 2.- Continued.

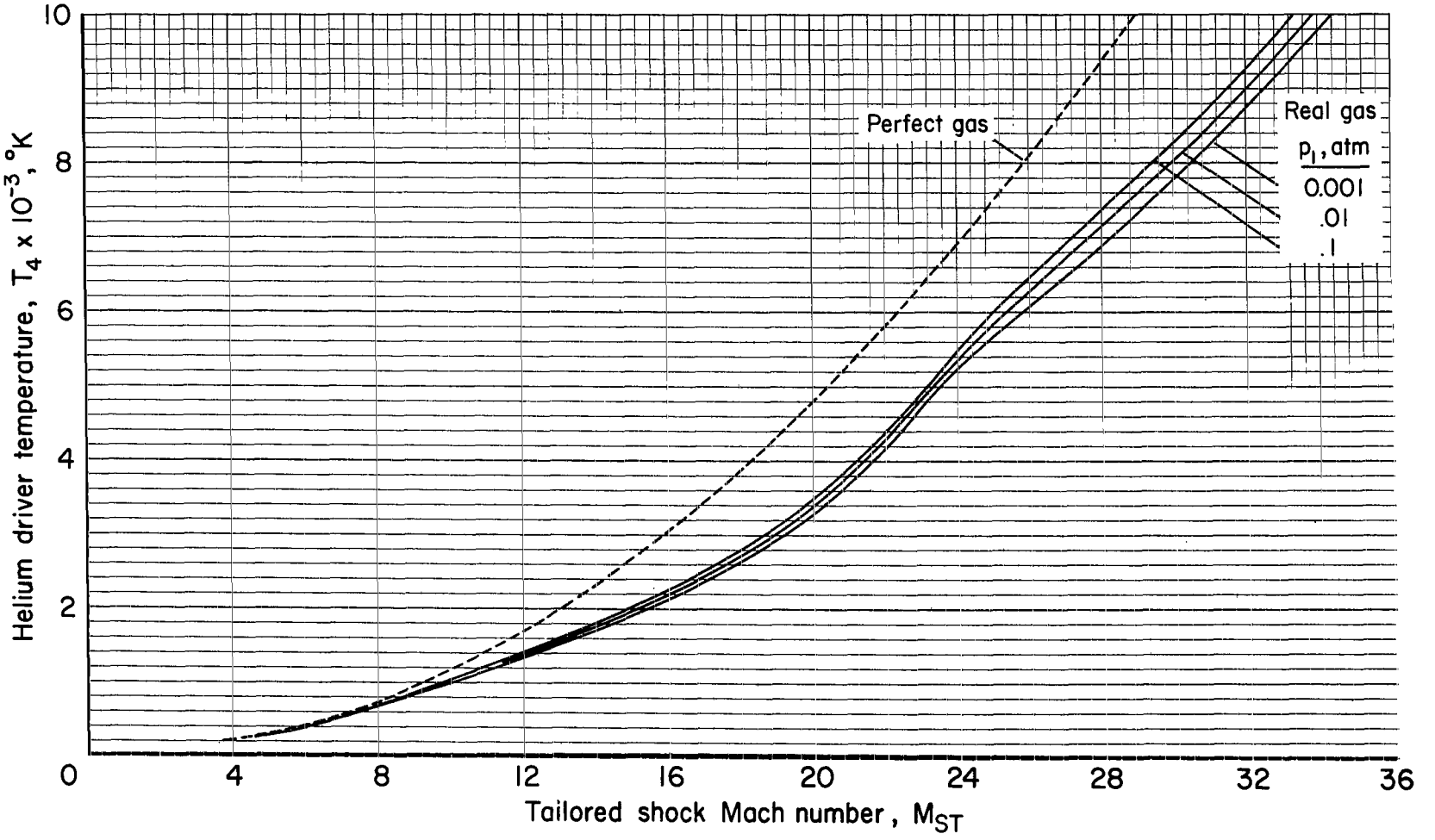

(c) Carbon dioxide.

Figure 2.- Continued.

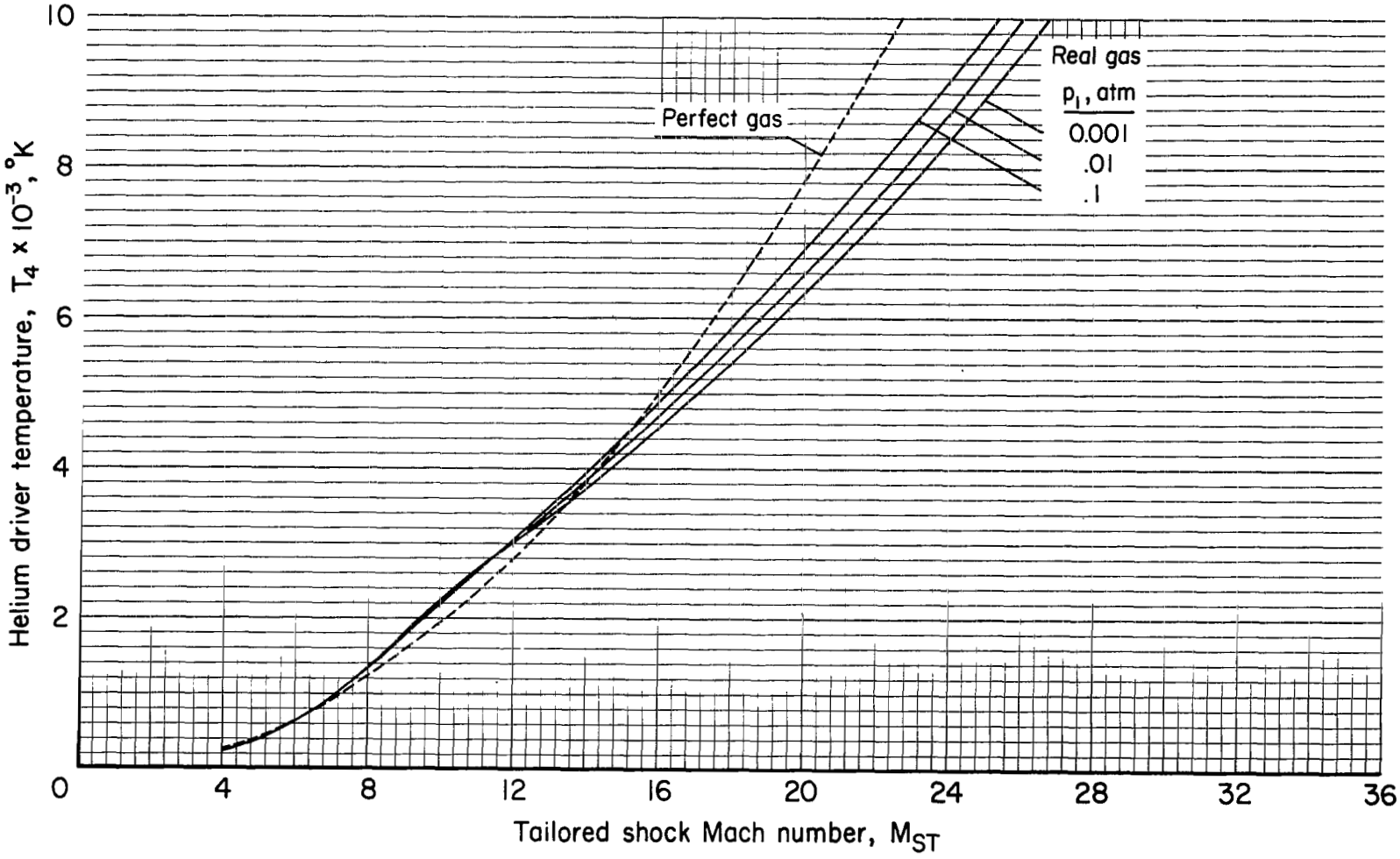

(d) Argon.

Figure 2.- Concluded.

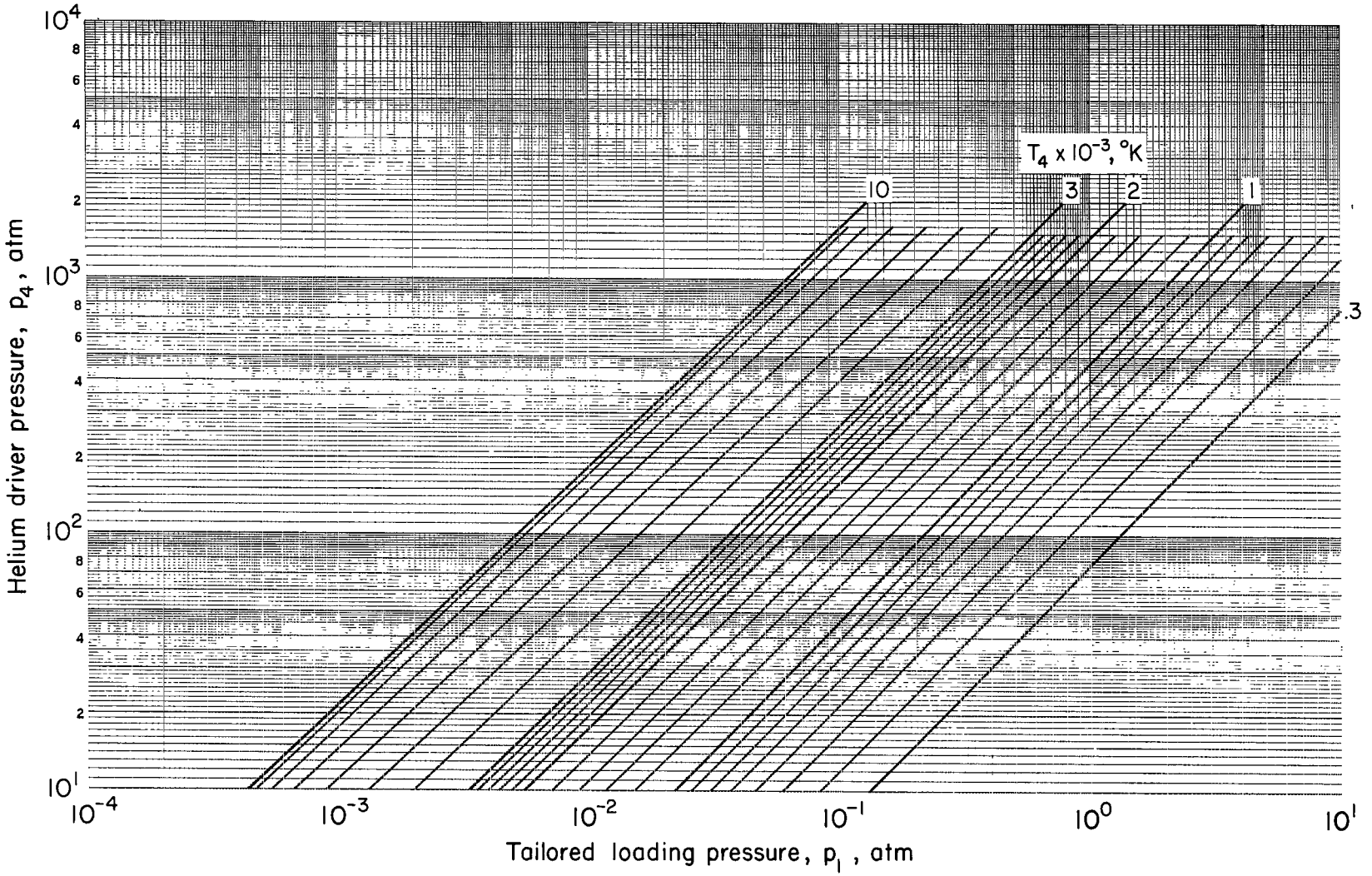

(a) Air.

Figure 3.- Initial pressure of test gas in the driven tube for a tailored reflected shock wave.

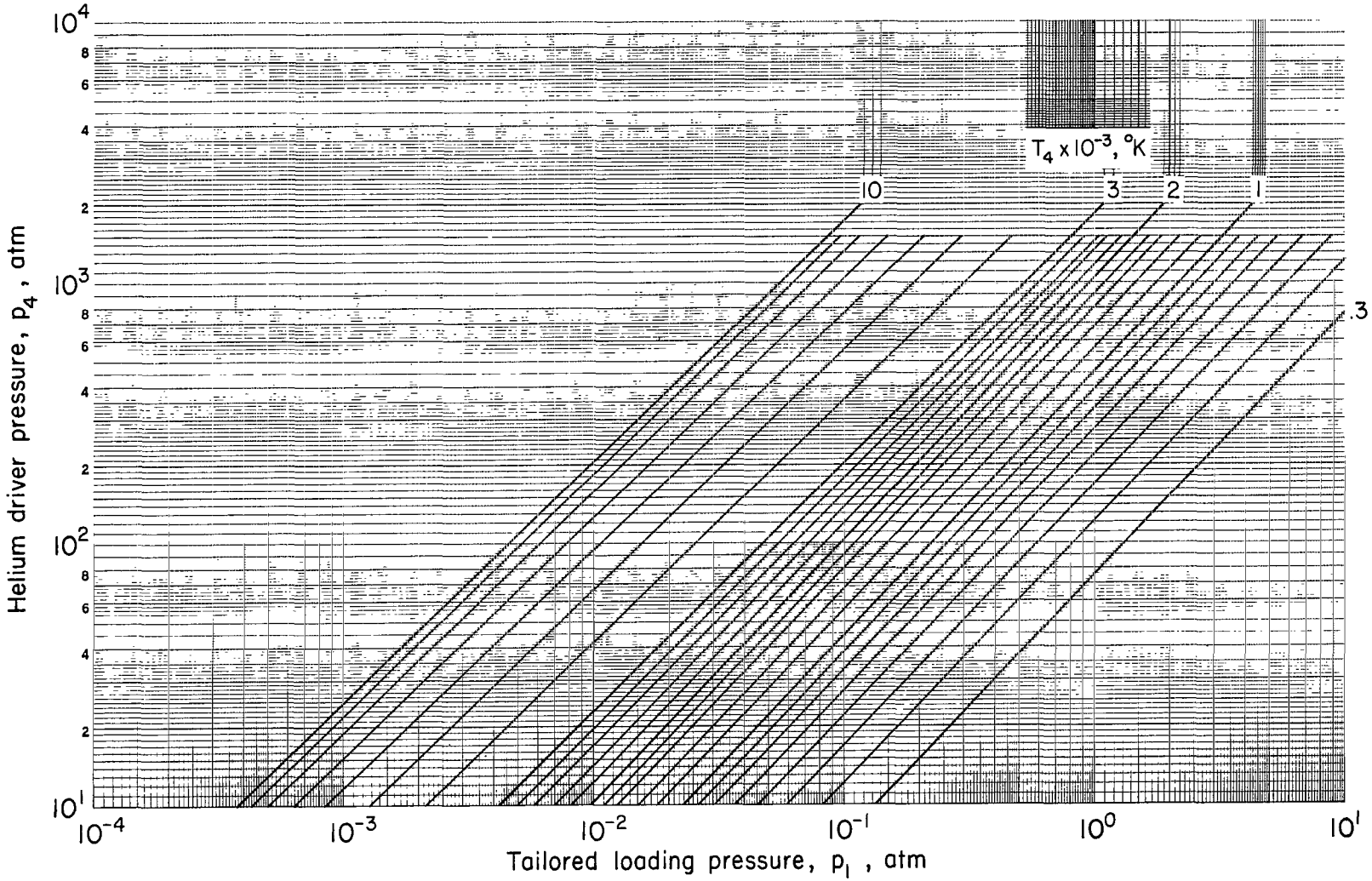

(b) Nitrogen.

Figure 3.- Continued.

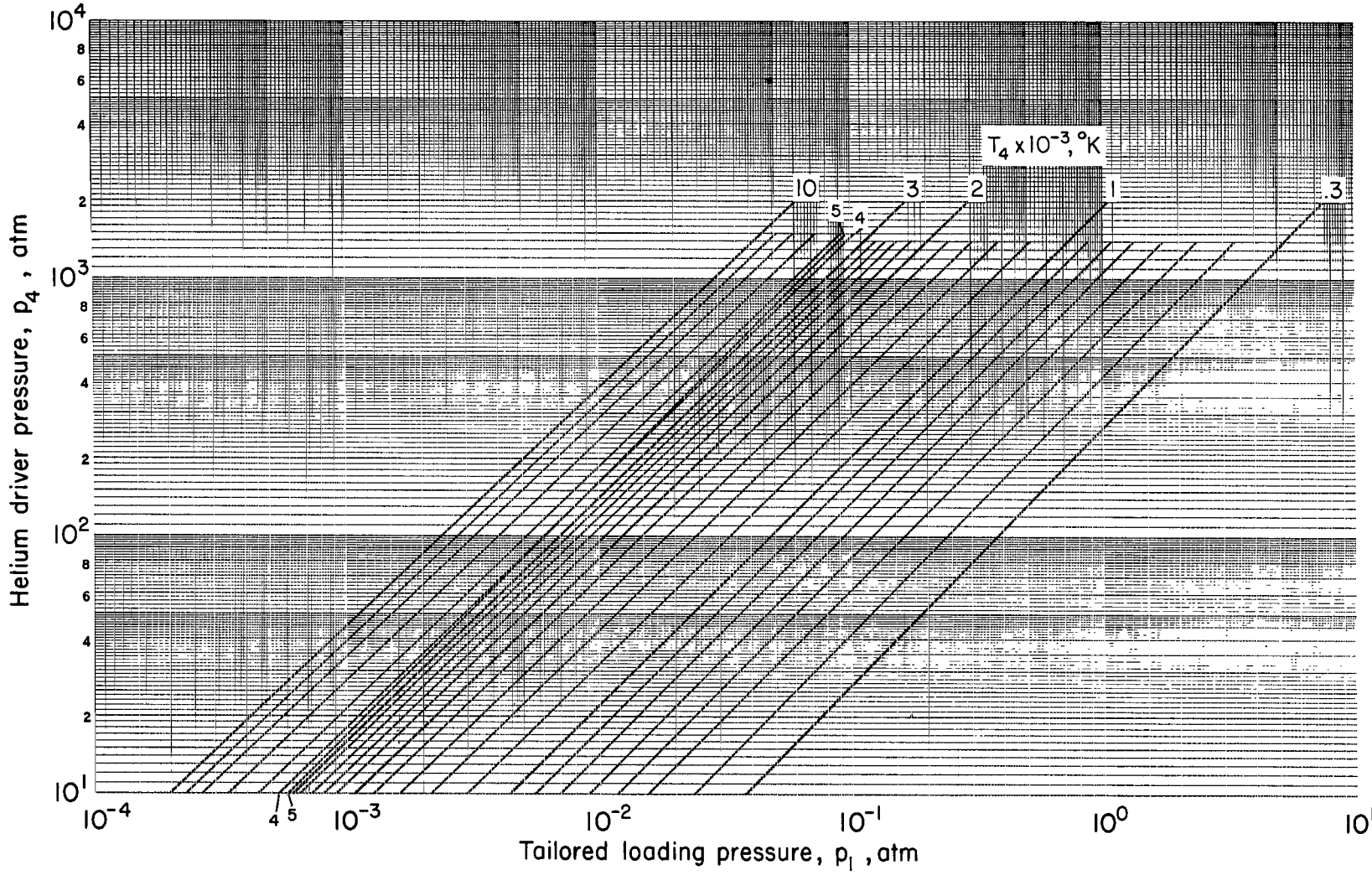

(c) Carbon dioxide.

Figure 3.- Continued.

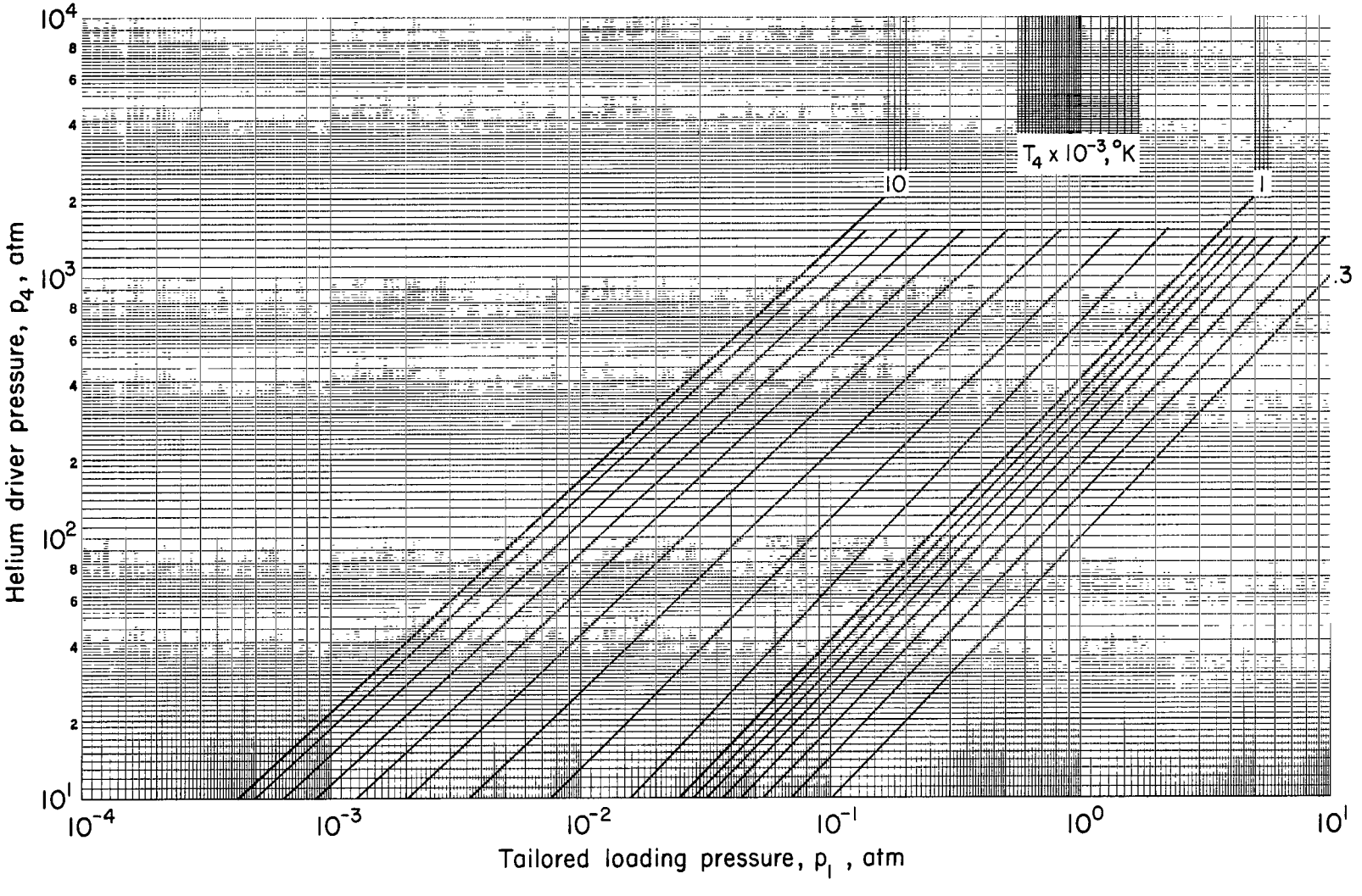

(d) Argon.

Figure 3.- Concluded.

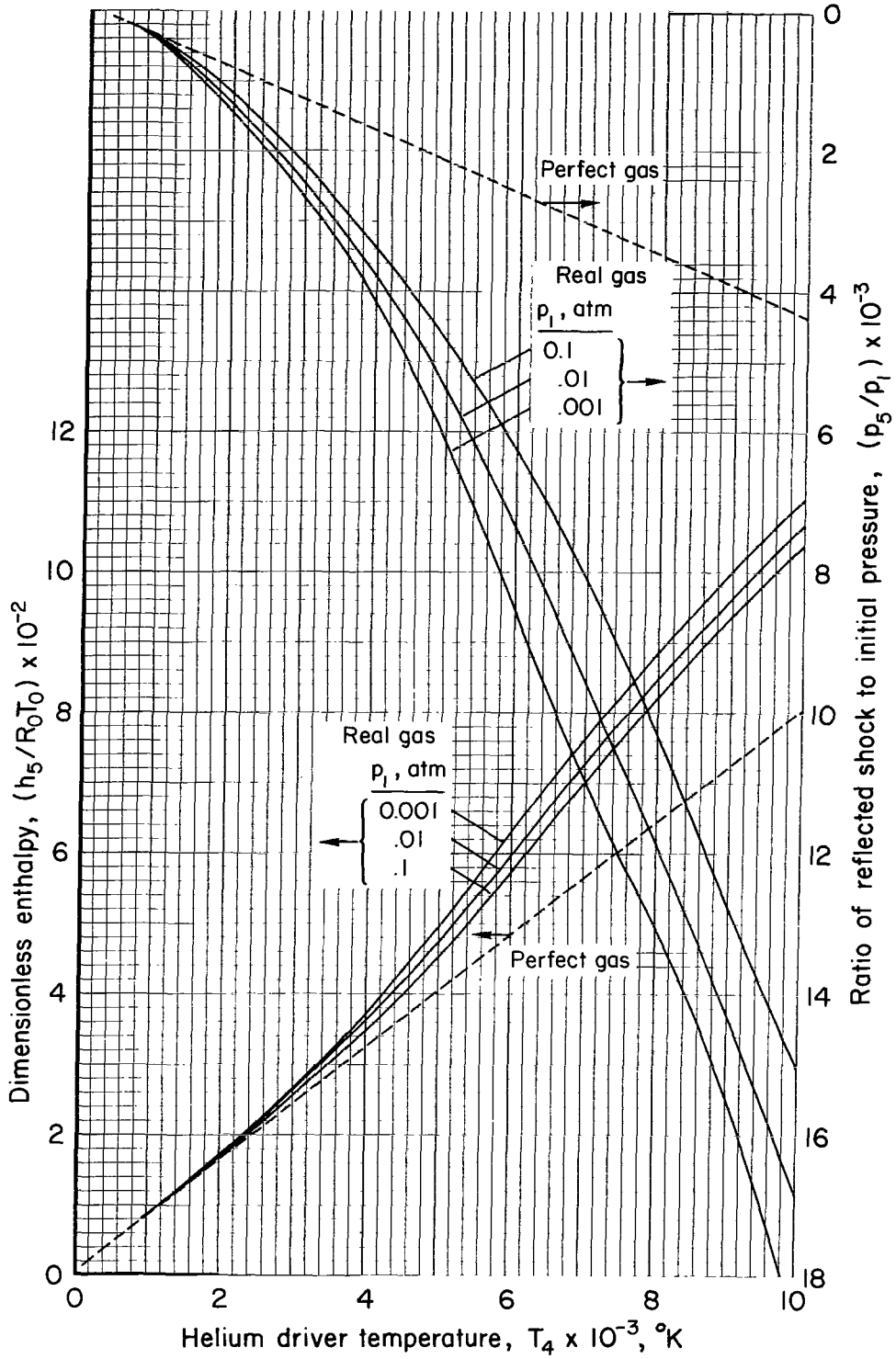

(a) Air.

Figure 4.- Reflected shock enthalpy and pressure for tailored conditions (P_4 not arbitrary).

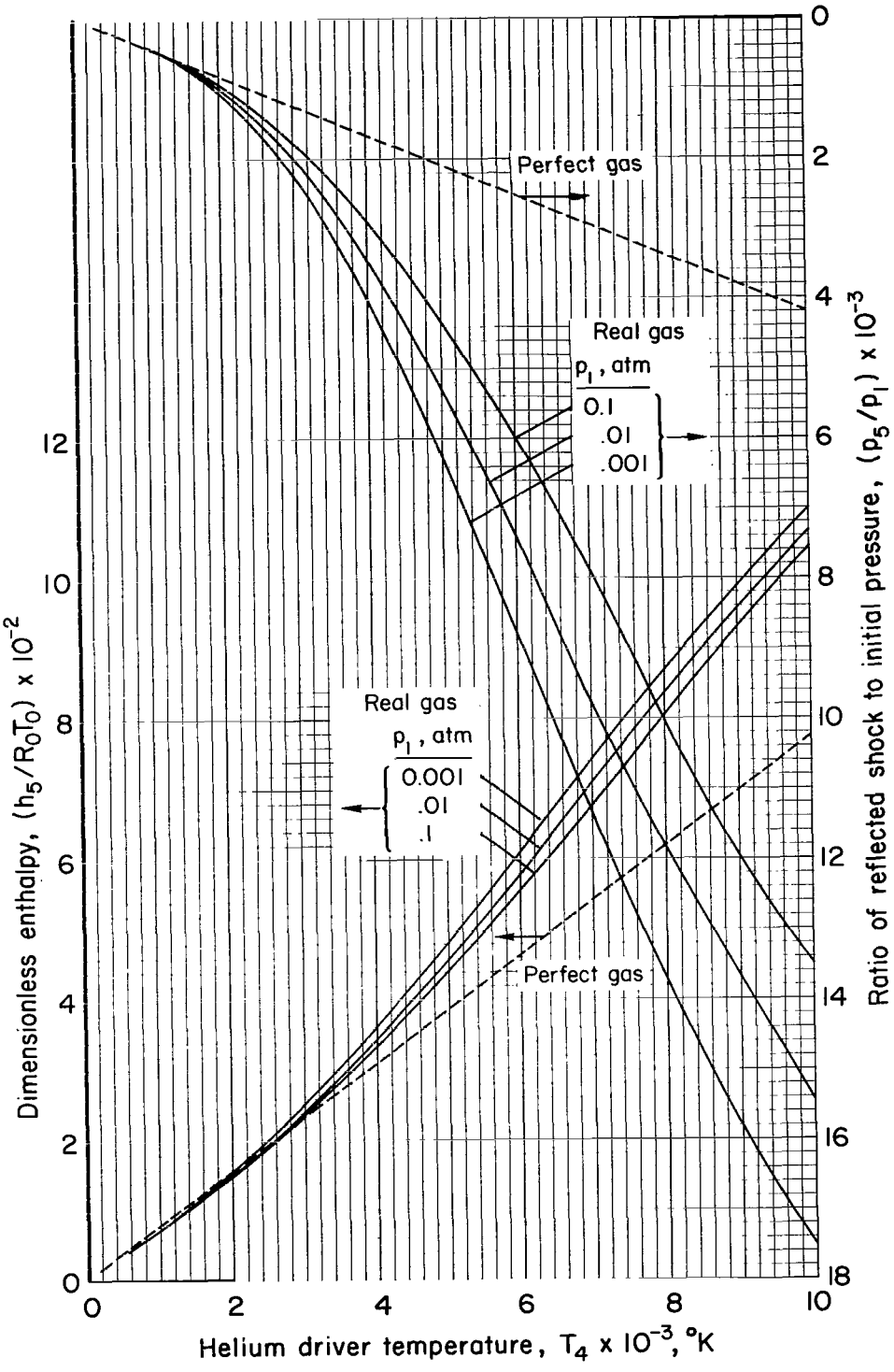

(b) Nitrogen.

Figure 4.- Continued.

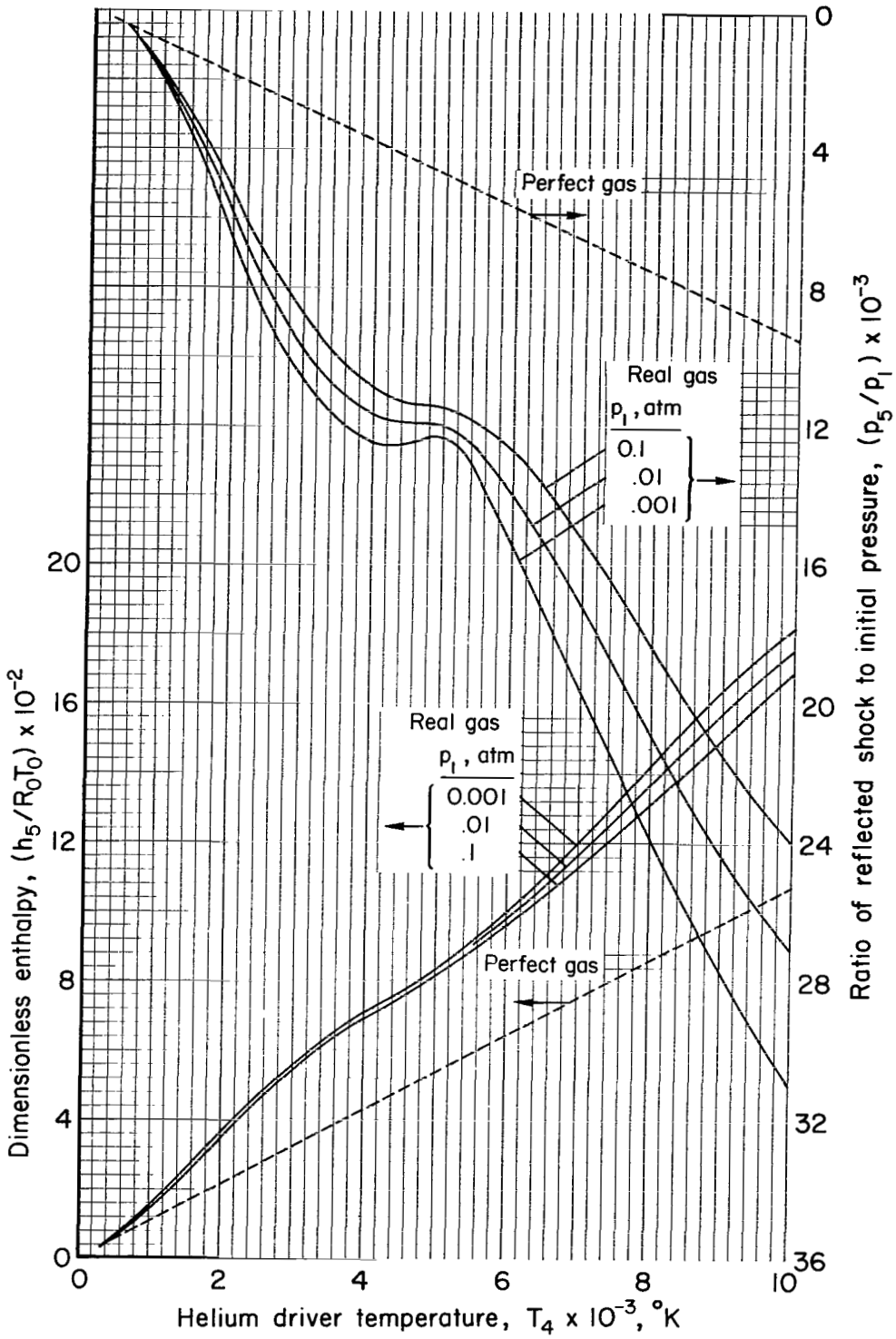

(c) Carbon dioxide.

Figure 4.- Continued.

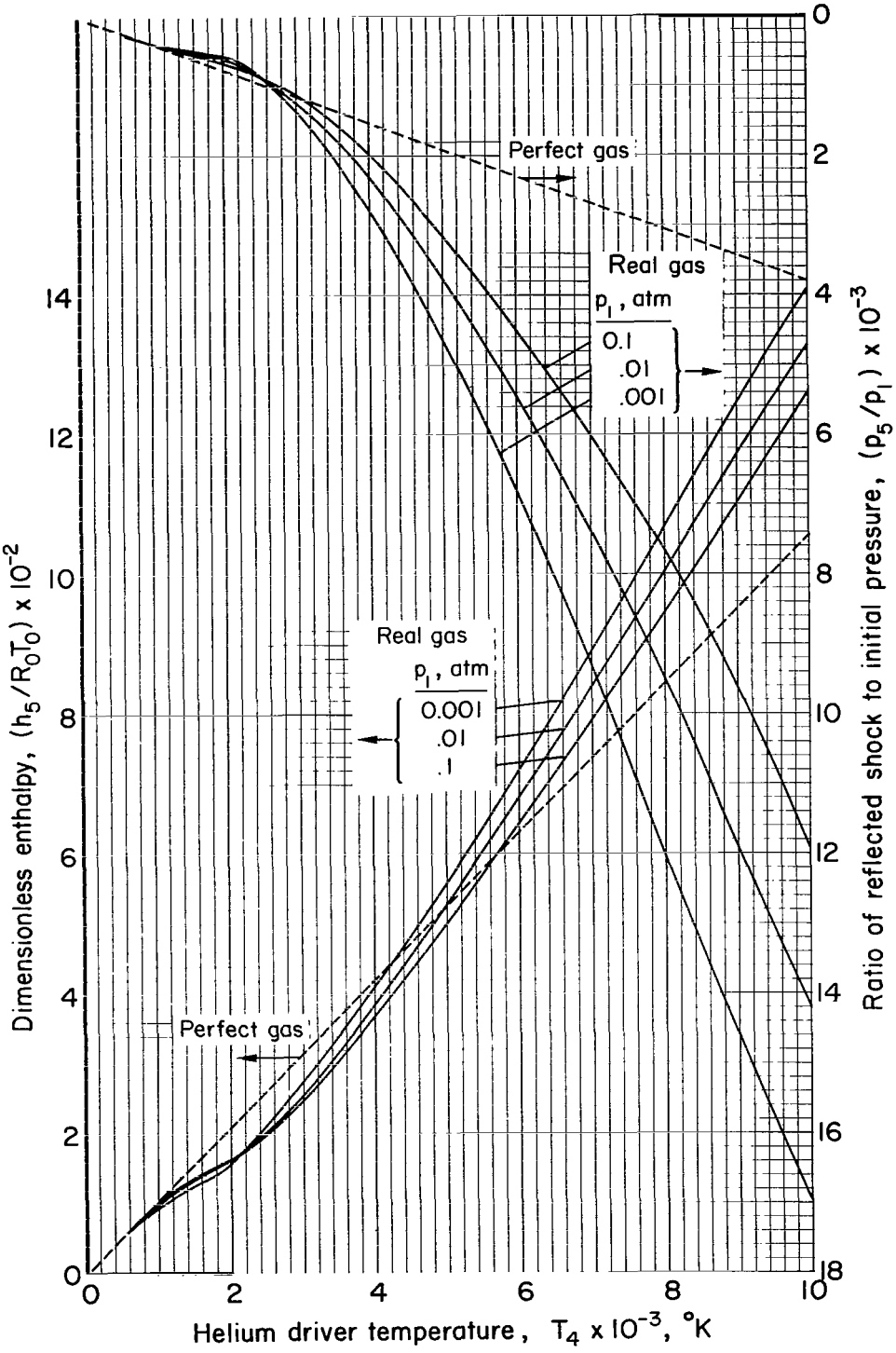

(d) Argon.

Figure 4.- Concluded.

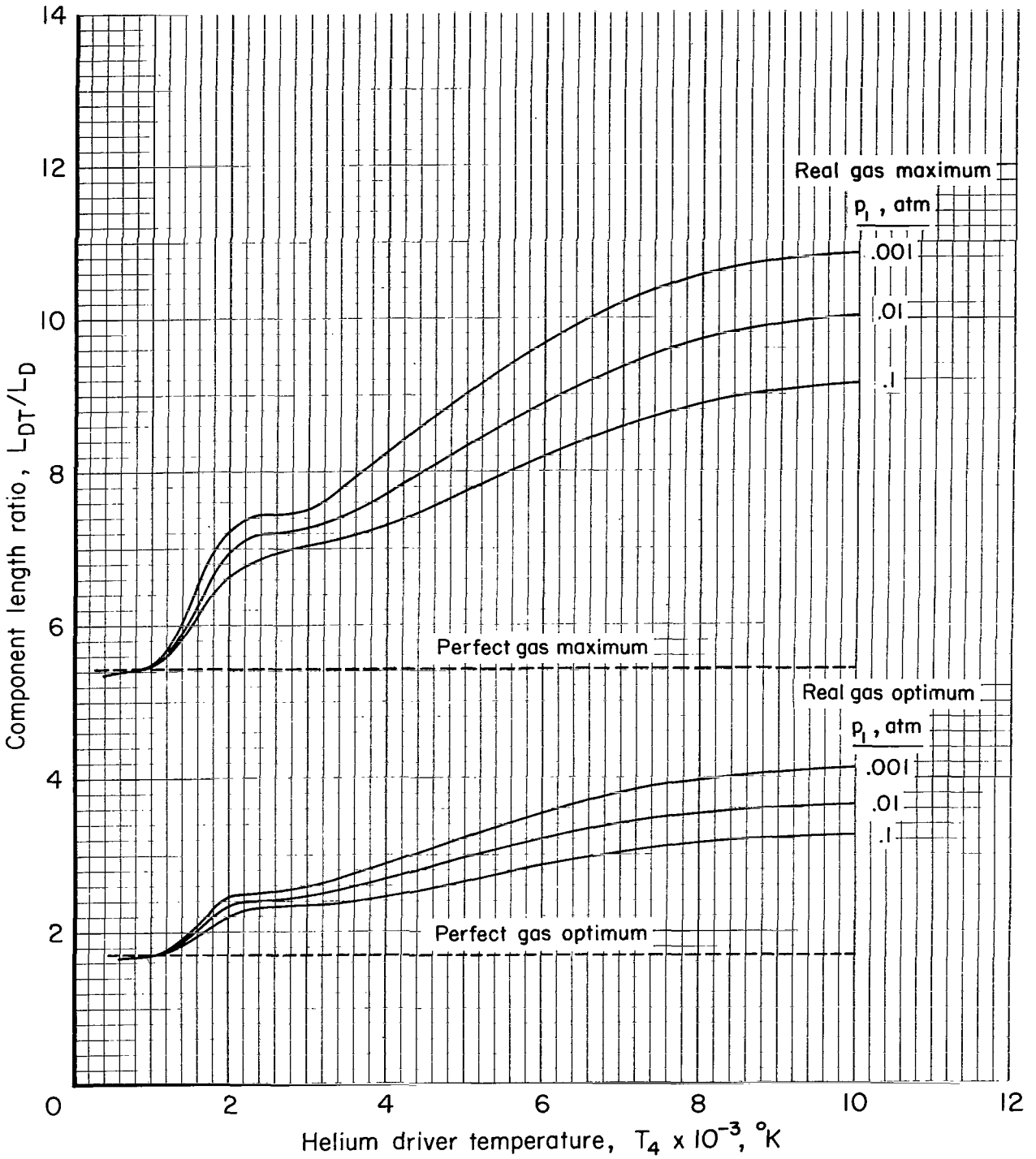

(a) Air.

Figure 5.- Shock tube component length ratios.

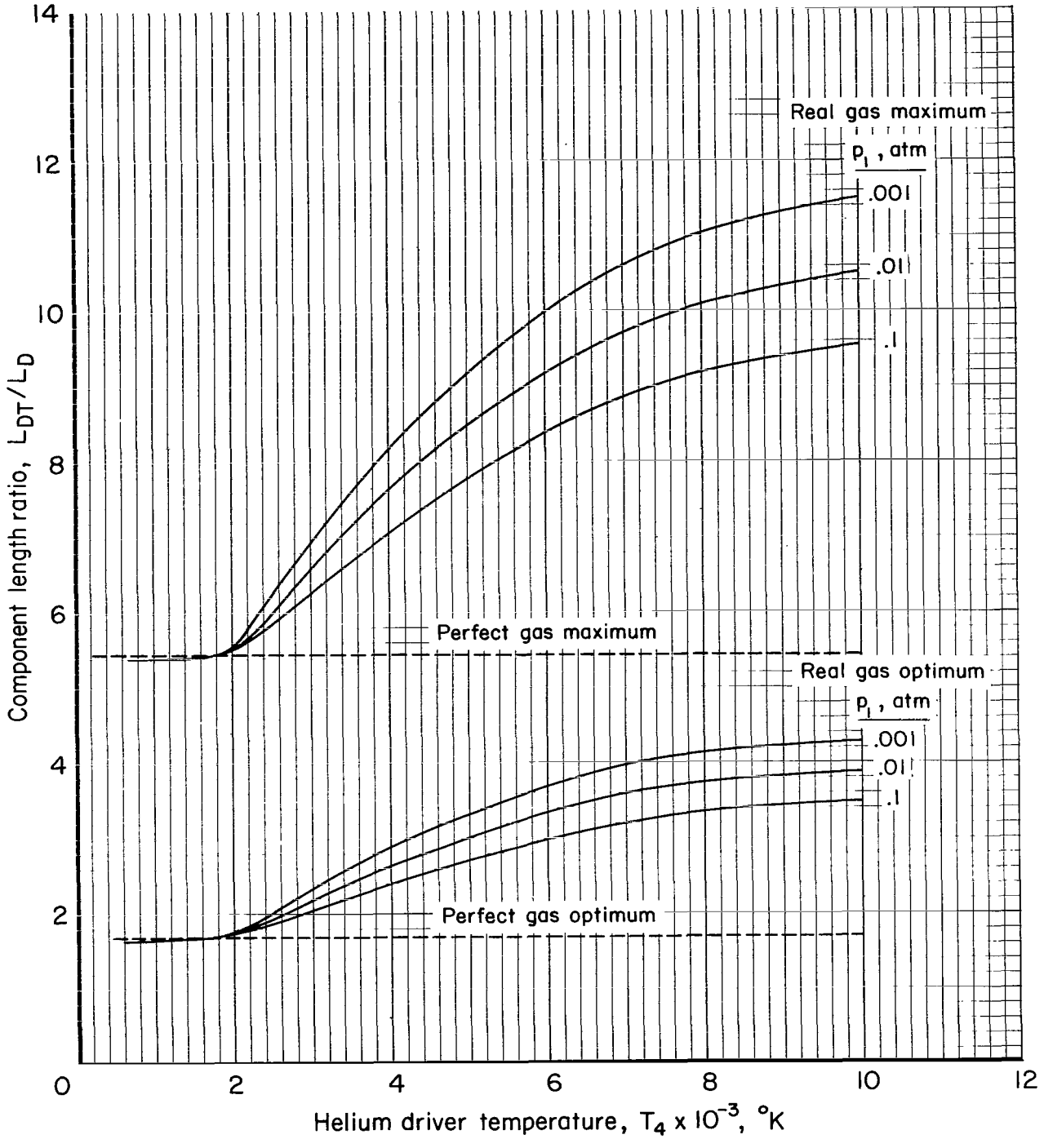

(b) Nitrogen.

Figure 5.- Continued.

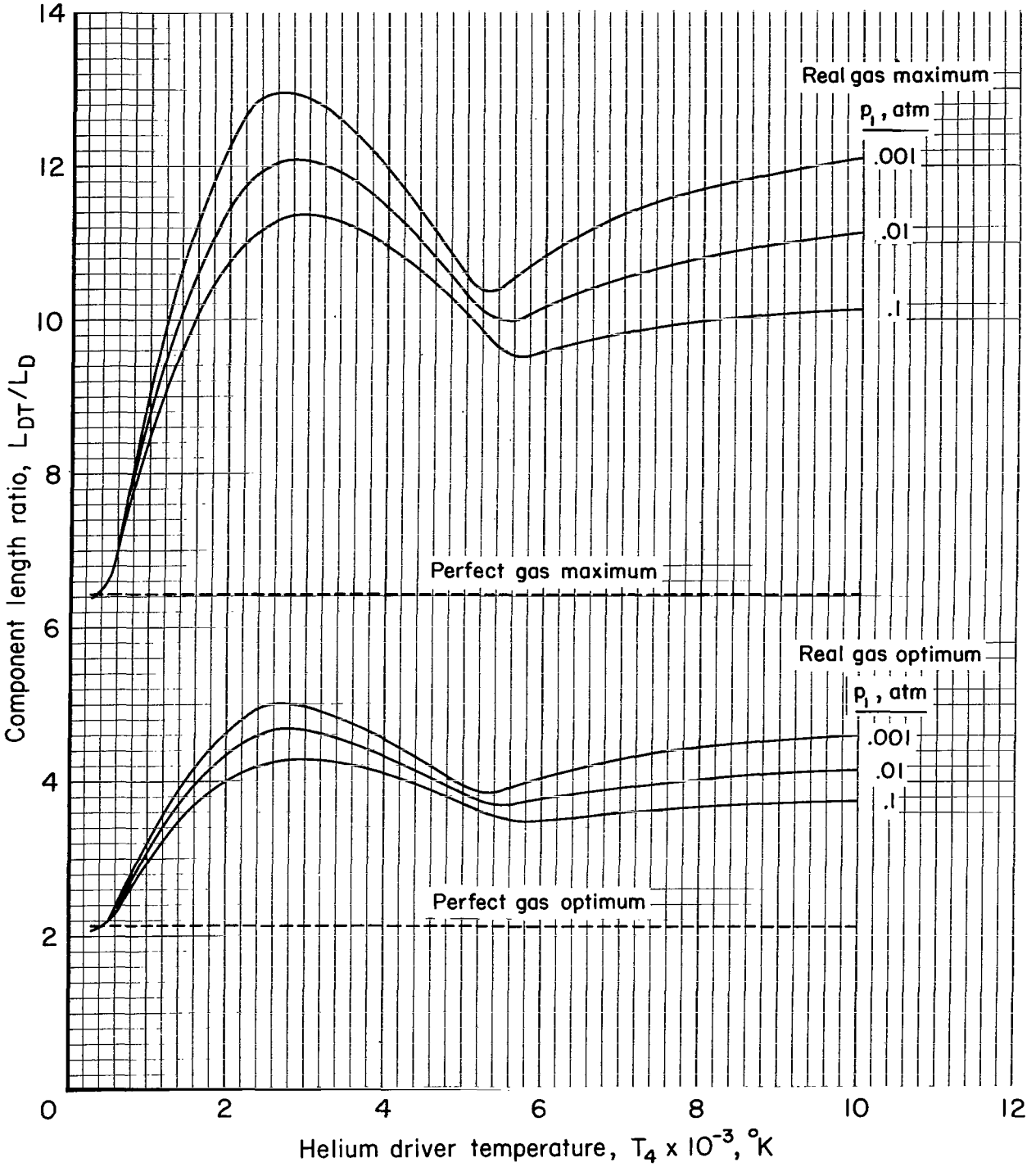

(c) Carbon dioxide.

Figure 5.- Continued.

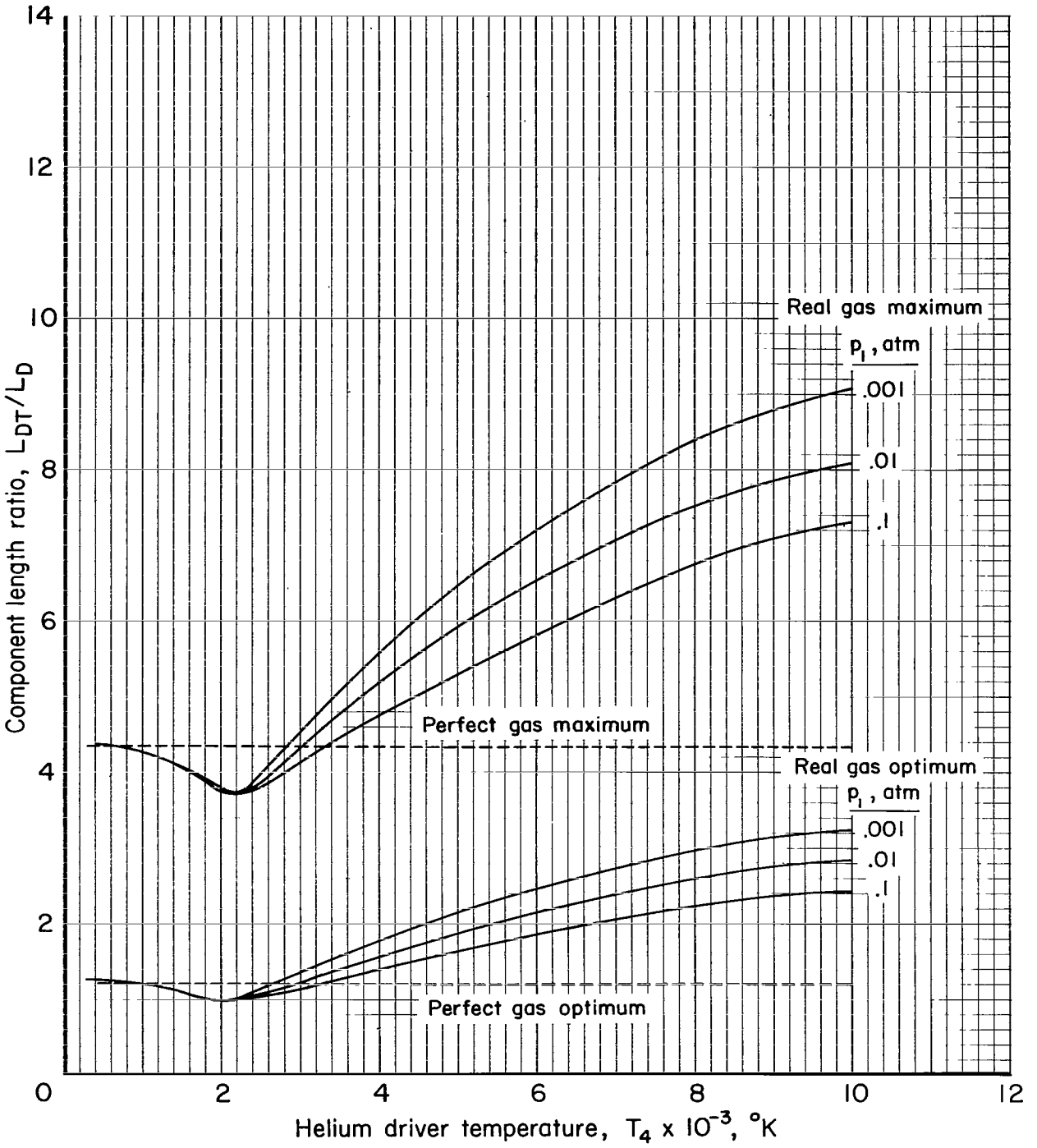

(d) Argon.

Figure 5.- Concluded.

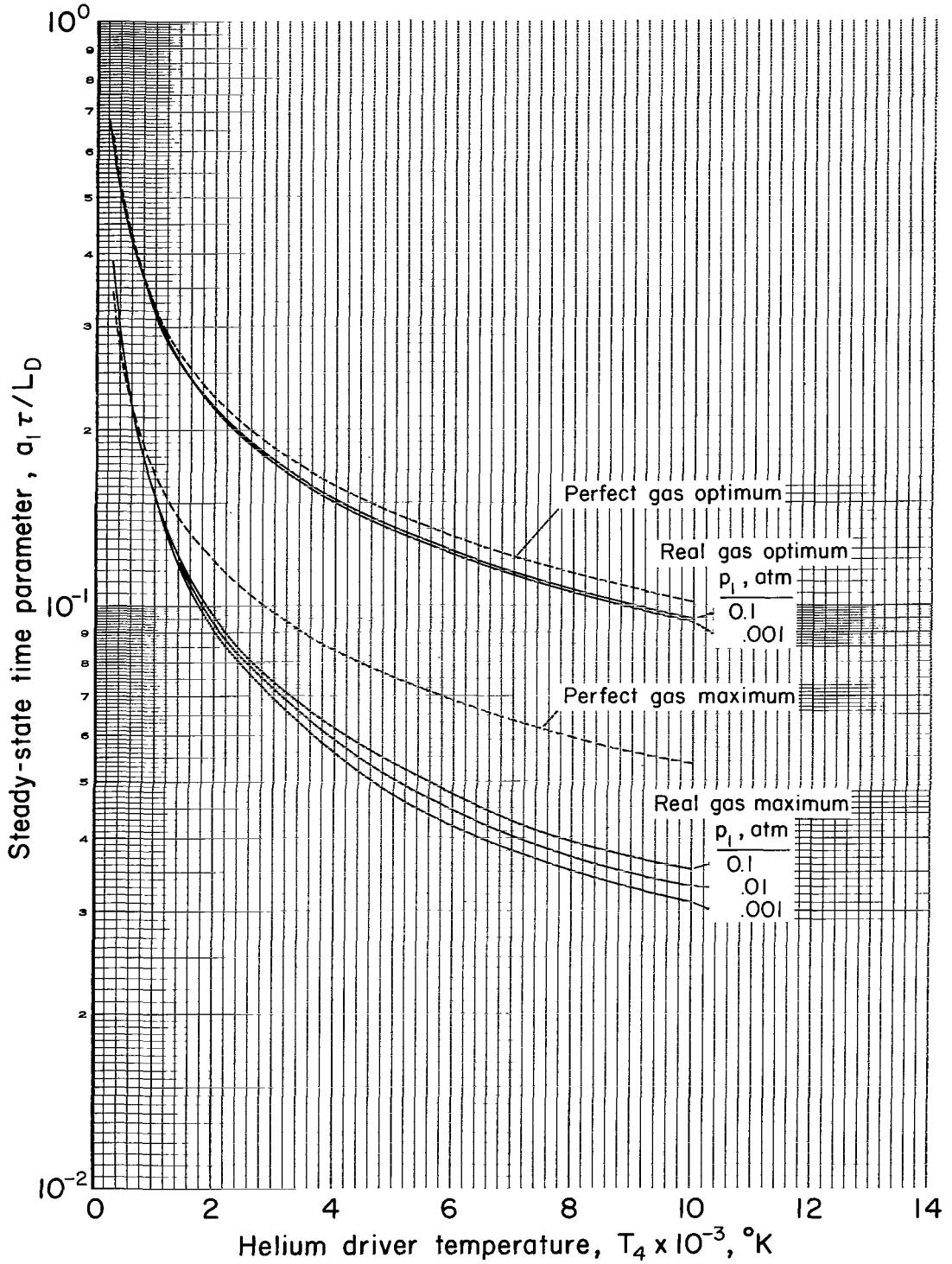

(a) Air.

Figure 6.- Steady-state time at tailored conditions; optimum and maximum L_{DT}/L_D ratios.

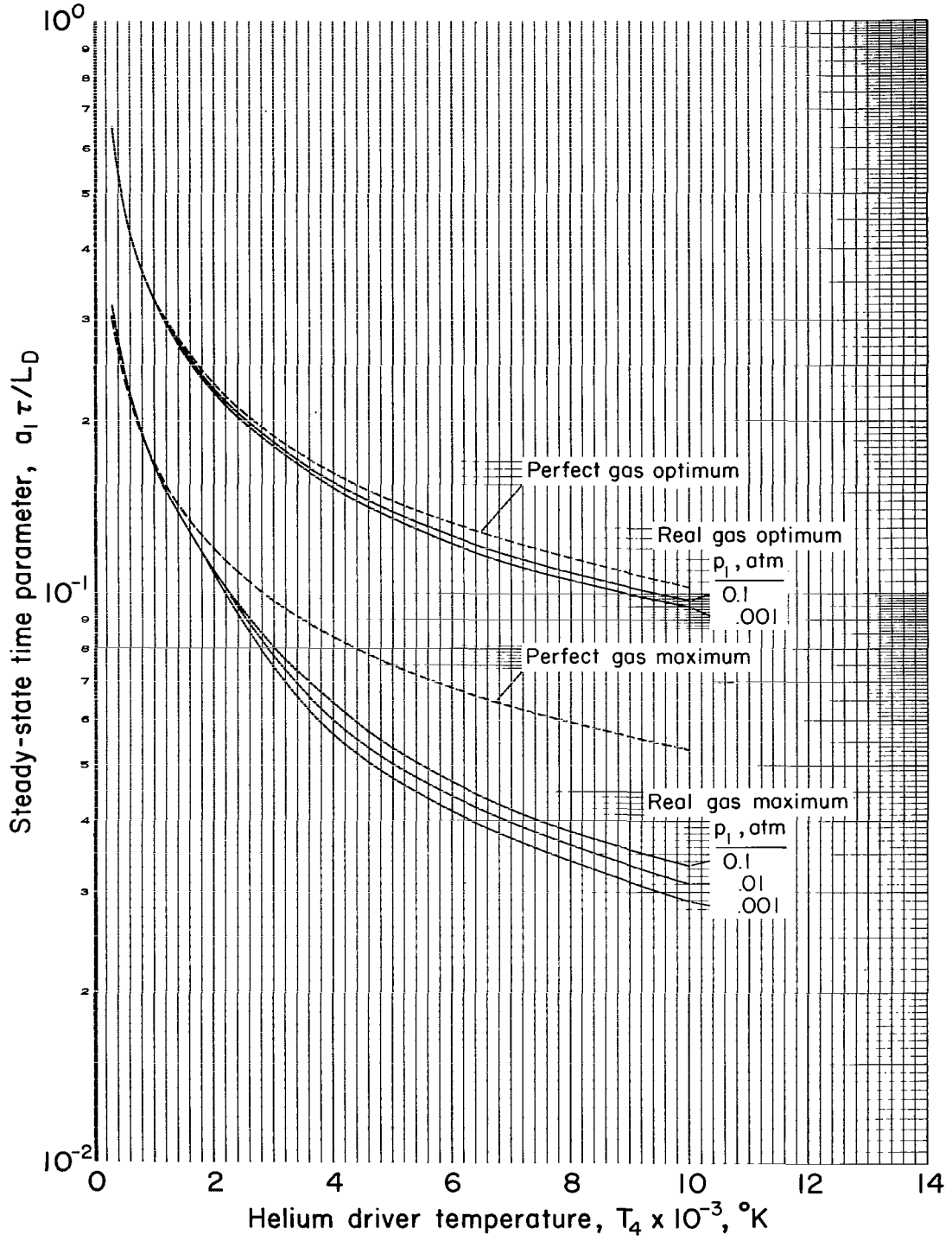

(b) Nitrogen.

Figure 6.- Continued.

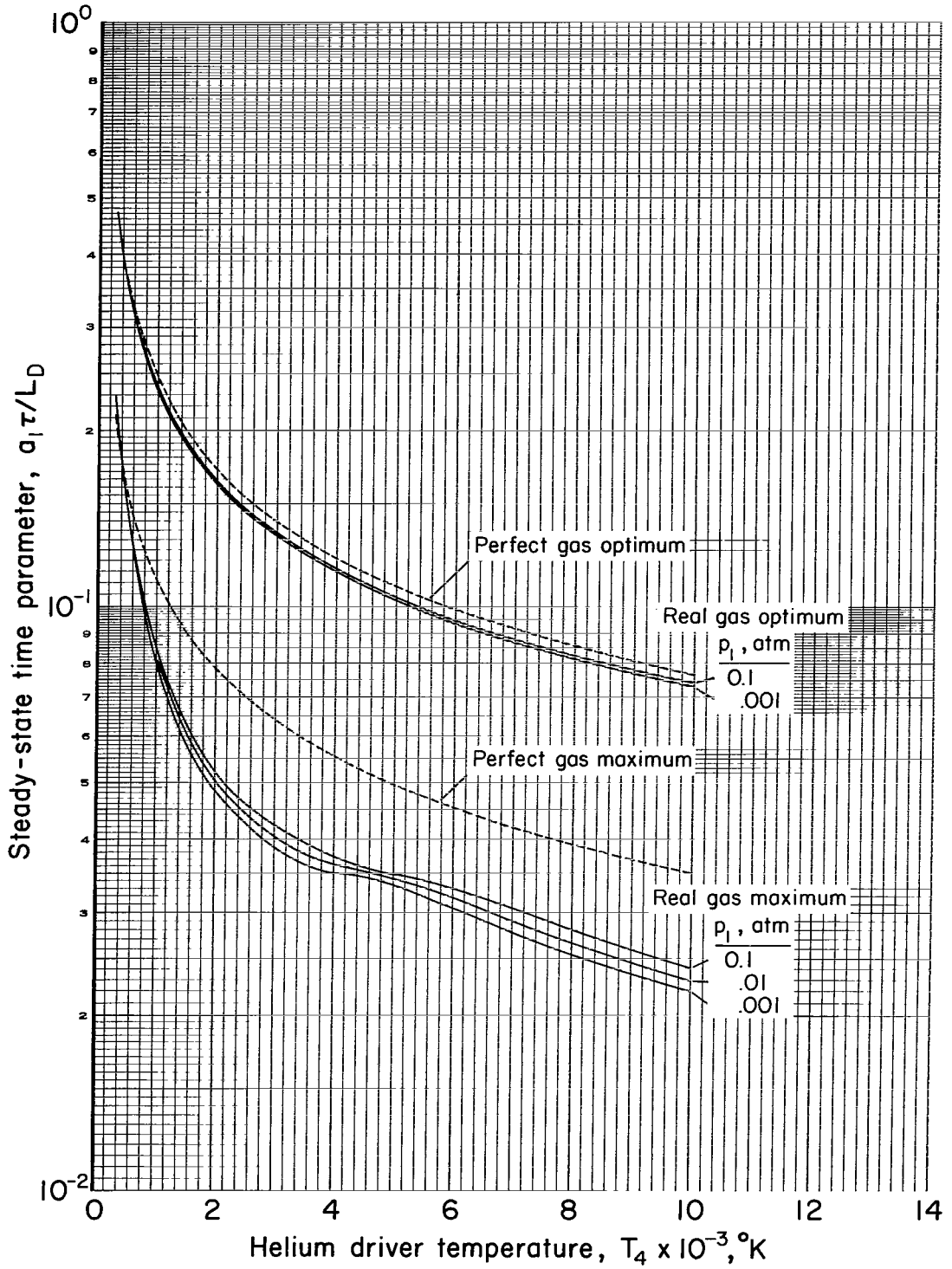

(c) Carbon dioxide.

Figure 6.- Continued.

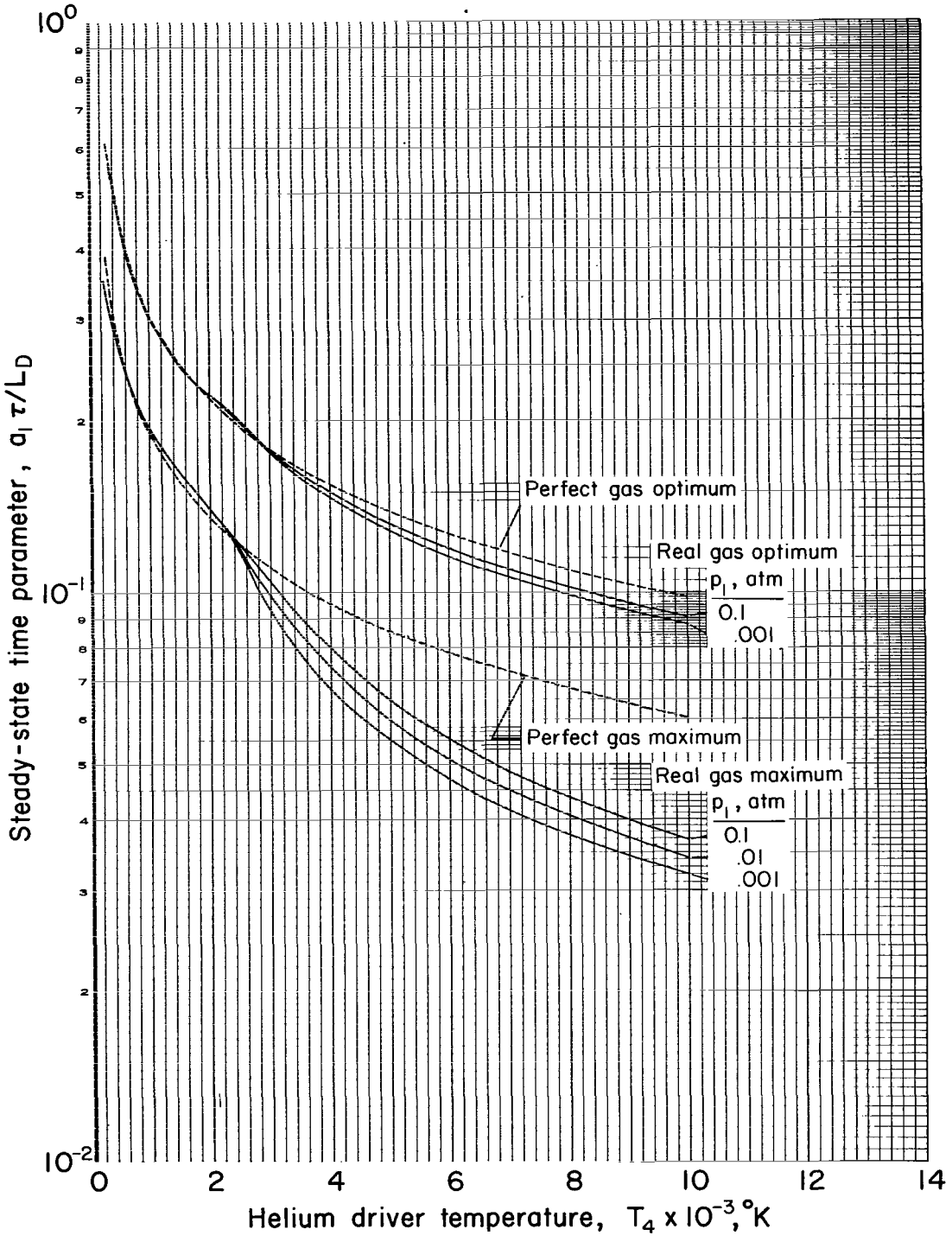

(d) Argon.

Figure 6.- Concluded.

"The aeronautical and space activities of the United States shall be conducted so as to contribute . . . to the expansion of human knowledge of phenomena in the atmosphere and space. The Administration shall provide for the widest practicable and appropriate dissemination of information concerning its activities and the results thereof."

—NATIONAL AERONAUTICS AND SPACE ACT OF 1958

NASA SCIENTIFIC AND TECHNICAL PUBLICATIONS

TECHNICAL REPORTS: Scientific and technical information considered important, complete, and a lasting contribution to existing knowledge.

TECHNICAL NOTES: Information less broad in scope but nevertheless of importance as a contribution to existing knowledge.

TECHNICAL MEMORANDUMS: Information receiving limited distribution because of preliminary data, security classification, or other reasons.

CONTRACTOR REPORTS: Technical information generated in connection with a NASA contract or grant and released under NASA auspices.

TECHNICAL TRANSLATIONS: Information published in a foreign language considered to merit NASA distribution in English.

TECHNICAL REPRINTS: Information derived from NASA activities and initially published in the form of journal articles.

SPECIAL PUBLICATIONS: Information derived from or of value to NASA activities but not necessarily reporting the results of individual NASA-programmed scientific efforts. Publications include conference proceedings, monographs, data compilations, handbooks, sourcebooks, and special bibliographies.

Details on the availability of these publications may be obtained from:

SCIENTIFIC AND TECHNICAL INFORMATION DIVISION

NATIONAL AERONAUTICS AND SPACE ADMINISTRATION

Washington, D.C. 20546